Epigenetic Studies of Mouse Preimplantation Embryos by Live-cell Imaging

A Dissertation Submitted to

the Graduate School of Life and Environmental Sciences,

the University of Tsukuba

in Partial Fulfillment of the Requirements

for the Degree of Doctor of Philosophy in Agricultural Science

(Doctoral Program in Life Sciences and Bioengineering)

Taiga YAMAZAKI

ABBREVIATIONS

BSA	bovine serum albumin
CENPB	centromere protein B
EGFP	enhanced green fluorescence protein
FRAP	fluorescence recovery after photobleaching
hCG	human chorionic gonadotropin
HP1β	heterochromatin protein 1β
ICSI	intra cytoplasmic sperm injection
IVF	*in vitro* fertilization
MBD	methyl CpG binding domain
MBD1	methyl CpG binding protein 1
mRFP	monomeric red fluorescence protein
NLS	nuclear localization signal
PAGE	polyacrylamide gel electrophoresis
PBS	phosphate-buffered saline
PCR	polymerase chain reaction
PMSG	pregnant mare's serum gonadotropin
ROI	region of interest
ROSI	round spermatid injection
SCNT	somatic cell nuclear transfer
SDS	sodium dodecyl sulfate
5mC	5-methylcytosine

CONTENTS

GENERAL INTRODUCTION

Fertilization, the union of sperm and egg to generate a new organism, is a critical process that bridges generations (Fig. 1). Following fertilization, the molecular and cellular changes take place in the eggs fused with the sperm (Yanagimachi, 1994). The metaphase II-arrested eggs resume second meiosis accompanying extrusion of the second polar body. The sperm nucleus is swollen, and the nucleoprotein protamine is substituted by histone (Yanagimachi, 1994). After the pronuclear formation, first DNA replication and *de novo* transcription occur, and then first mitosis starts (Aoki et al., 1997; Bouniol et al., 1995). In addition to the structural changes of chromatin, the DNA methylation state is genome-widely changed (Fig.1). A rapid loss of DNA methylation paternal-specifically takes place without DNA replication (termed active demethylation) (Mayer et al., 2000; Santos et al., 2002). While active demethylation unsymmetrically occurs in the paternal genome of 1-cell embryos, stepwise DNA demethylation is continued until the morula-blastocyst stage (Santos et al., 2002). The observed DNA demethylation pattern is thought to result from the absence of DNA methyltransferase1 in the nucleus of preimplantation embryos (Doherty et al., 2002; Howell et al., 2001; Ratnam et al., 2002).

The cytosine residue of CpG dinucleotide in chromosomal DNA is known to be methylated at the C-5 position (Ng et al., 1999; Razin and Riggs, 1908). The methylcytosine (5mC) plays a central role in transcriptional repression by recruiting methyl-CpG binding proteins and other transcriptional repressors (Li, 2002). Thus, DNA demethylation of the male and female genomes in the 1-cell embryo may be important for resetting the

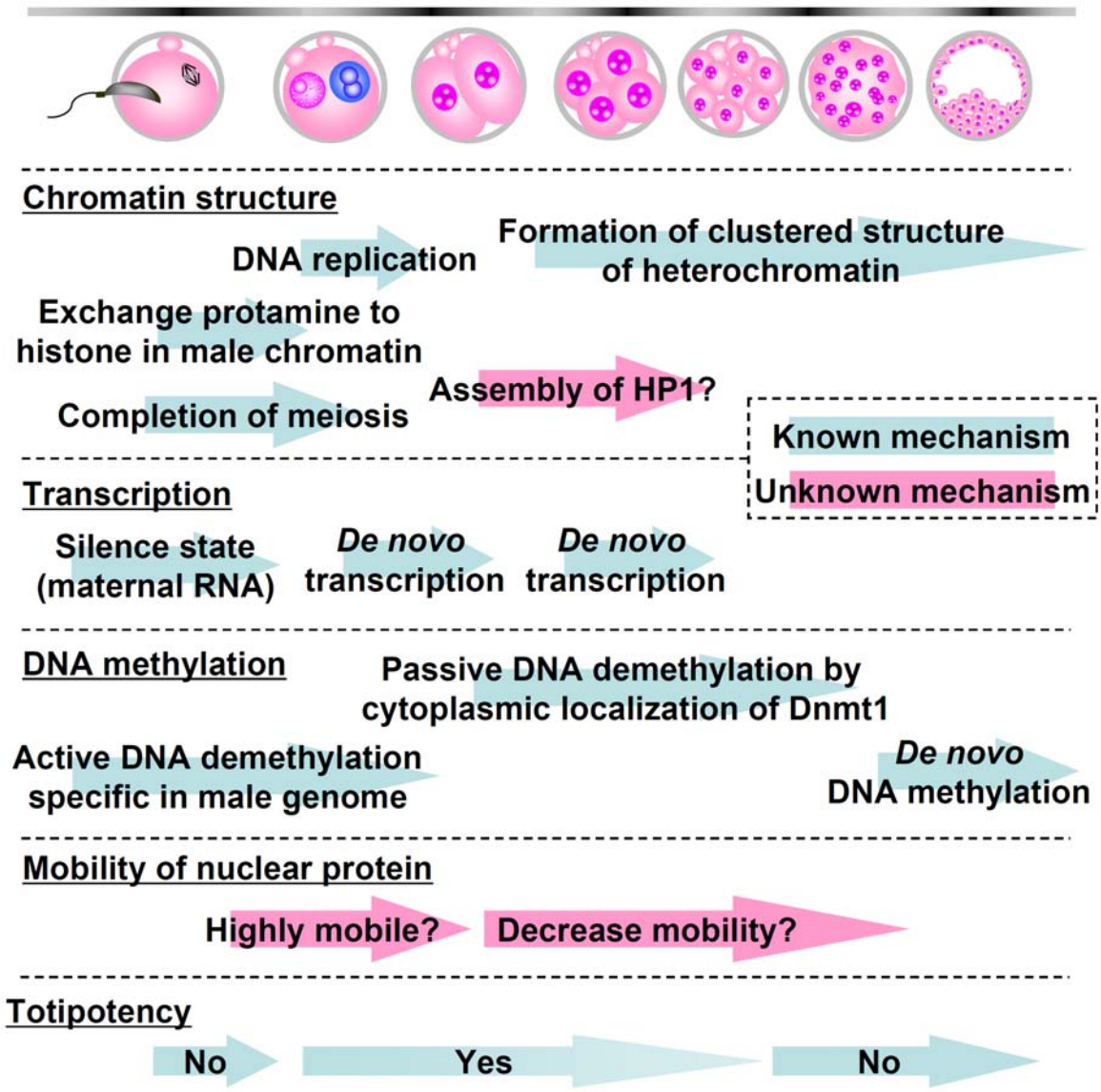

Fig. 1. Molecular and cellular events occur during preimplantation development. After fertilization, dynamic changes of chromatin structure, transcriptional activity, and epigenetic modifications take place in parallel. In fertilized embryos, protamine, a major nucleoprotein of sperm, is substituted by maternally stored histone, and then meiosis is completed. DNA replication, DNA demethylation, and *de novo* transcription occur after pronuclear formation. Totipotency of early embryos may be acquired at the 2-cell stage, and may be lost at the 8-cell stage. The known and unknown mechanisms are shown by blue and pink arrows, respectively.

Table 1. Current reports about DNA methylation during preimplantation development

Author	Experimental design	Genes analyzed	Published year	Journal
Mayer, W. *et al*.	Immunostaining	-	2000	Nature
Oswald, J. *et al*.	Bisulfite sequencing	*Igf* 2, α-actin, *myl*-C	2000	Curr. Biol.
Barton, S.C. *et al*.	Immunostaining	-	2001	HMG
Dean, W. *et al*.	Immunostaining	-	2001	PNAS
Kang, Y.K. et al.	Bisulfite sequencing	Repeat sequences	2001	Nat. Genet.
Santos, F. *et al*.	Immunostaining	-	2002	Dev. Biol.
Wilmut, I. *et al*.	Immunostaining	-	2002	Nature
Lane, N. *et al*.	Bisulfite sequencing	*Line 1, IAP*	2003	Genesis
Beaujean N. *et al.*	Immunostaining	-	2004	Curr. Biol.
Beaujean N. *et al.*	Immunostaining	-	2004	PNAS
Kim S.H. *et al.*	Bisulfite sequencing	Repeat sequences	2004	BBRC
Beaujean N. *et al*.	Immunostaining	-	2004	Biol. Reprod.
Ko Y.G. *et al*.	Bisulfite sequencing	*Dnmt1o*	2005	JBC
Imamura T. *et al.*	Bisulfite sequencing	*Peg1/ Mest*	2005	JBC
Martin C. *et al.*	Immunostaining	-	2006	Dev. Biol.
Hiuma H. *et al.*	Bisulfite sequencing	*Dlk1-Gtl2*	2007	FEBS Let.
Nakamura T. *et al.*	Immunostaining	-	2007	Nat. Genet.
Yoshida N. *et al.*	Immunostaining	-	2007	Dev. Biol.

gene expression profiles unique in the sperm and eggs (Fulka et al., 2004). It is also interesting that the totipotency of embryos is acquired only after fertilization. Until the 4-cell stage, the blastomeres have been demonstrated to support independently the full-term development from nuclear transfer embryos using enucleated fertilized embryos as recipients, but the 8-cell embryos have no totipotency (McGrath and Solter, 1983; Tsunoda et al., 1987). It is thus conceivable that the process of preimplantation development may provide a unique opportunity to allow the sperm and egg to loose the characteristics as germ cells and to acquire a temporal totipotency. Although the answer to the question how cells acquire the totipotency has not yet been obtained at present, the success of somatic cell nuclear transfer (SCNT) appears to give us some hints. Even though cells commit to the cell lineages other than the germ cell lineage, the ontogeny is supported by introducing the nucleus into the enucleated unfertilized eggs (Wakayama et al., 1998; Wilmut et al., 1997). This fact leads to the probability that the reversibility is present in cellular differentiation that is accompanied by epigenetic changes without the rearrangement of DNA sequence; some epigenetic changes in the process of fertilization and preimplantation development may govern the “nuclear reprogramming” that supports the totipotency.

The molecular mechanism of the post-fertilization events remains unclear, because biochemical studies using mammalian embryos have inherent difficulties (Mager and Bartolomei, 2005). Only a small number of cells are prepared at once, and there is no line of cultured cells. For these reasons, immunostaining technique is widely utilized to examine the epigenetic changes using fixed embryos (Table 1). On the other hand, green fluorescence protein (GFP)-based fluorescent imaging of living cells is thought to be a

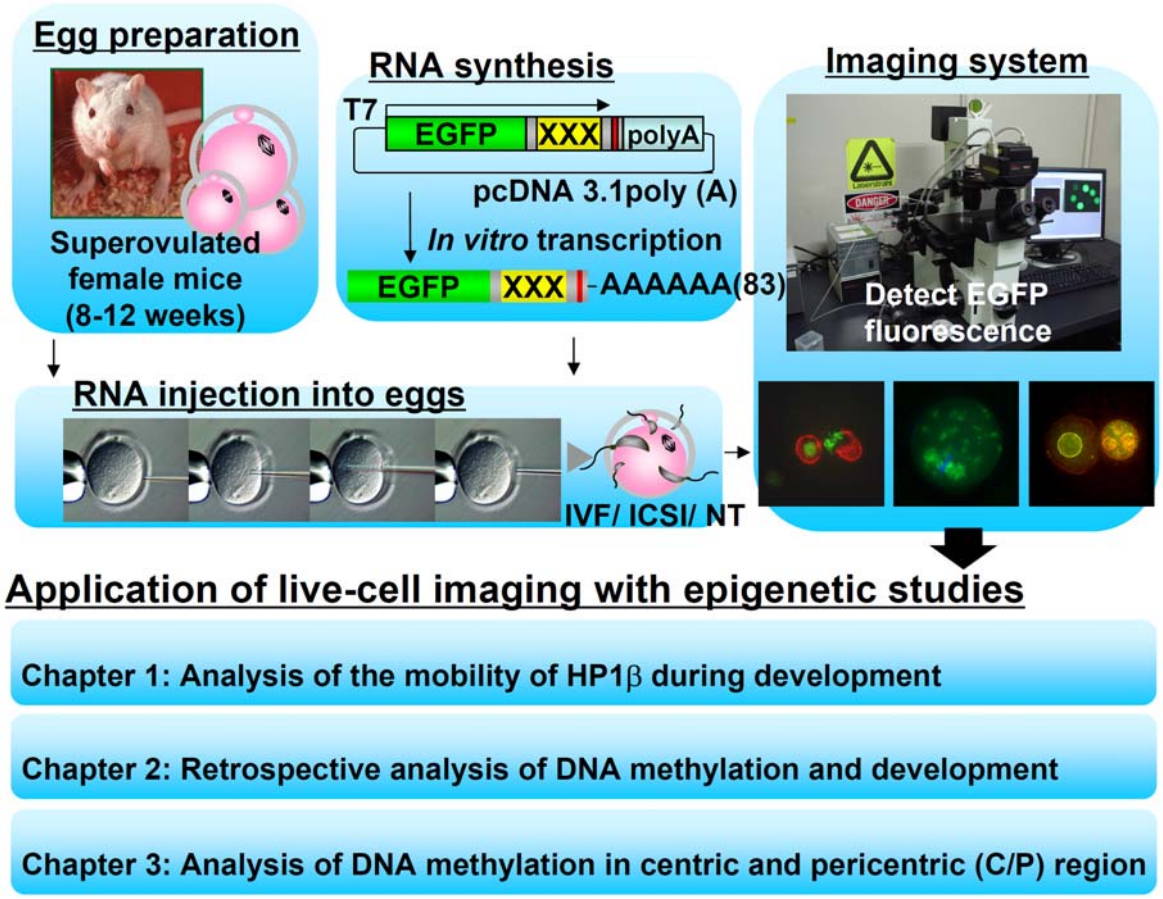

Fig. 2. Experimental scheme of EGFP-based live-cell imaging of preimplantation embryos.

Live-cell imaging is comprised of 4 steps. 1. Egg preparation from female mice. 2. Construction of expression plasmids encoding EGFP fusion proteins *in vitro*, and RNA synthesis by *in vitro* transcription using the linearized plasmids as templates. 3. Microinjection of the RNAs containing a Cap analog and poly(A) tail into the cytoplasm of fertilized or unfertilized eggs. 4. Detection of EGFP fluorescence in preimplantation embryos. FRAP analysis of EGFP-HP1β using 1-cell and 4-cell embryos, retrospective analysis of DNA methylation in ROSI embryos, and analysis of DNA methylation in centric and pericentric (C/P) regions using various germline cells or SCNT embryos have been performed in Chapters 1, 2, and 3, respectively.

powerful tool to understand the molecular basis of fertilization and preimplantation development (Kurotaki et al., 2007; Plusa et al., 2005). Thus, as shown in Fig. 2, I have recently developed a novel live-cell imaging technique using *in vitro* synthesized RNA (Yamagata et al., 2005). The outline of the imaging system is as follows:

1 Construction of expression plasmids encoding EGFP fusion proteins *in vitro*.
2 *In vitro* transcription (RNA synthesis) using the linearized plasmids as templates under the control of T7 promoter.
3 Microinjection of the RNAs containing a Cap analog and poly(A) tail into the cytoplasm of fertilized or unfertilized eggs.
4 Detection of EGFP fluorescence in preimplantation embryos.

The aim of this study is to understand the epigenetic mechanism underlying the nuclear reprogramming of preimplantation embryos. Live-cell imaging, which enables us to acquire 4-dimentional information, is applied. In chapter I, I have analyzed the molecular dynamics of HP1β, a major component of heterochromatin, in mouse early embryos using FRAP analysis. In chapter II, I have developed the method for detection of DNA methylation in the nucleus of living cells, and analyzed a direct correlation between DNA methylation and preimplantation development in ROSI embryos. Moreover, in chapter III, I have analyzed DNA methylation of the centric and pericentric regions of various germline cells and SCNT embryos.

CHAPTER I

Molecular Dynamics of Heterochromatin Protein 1β, HP1β, During Mouse Preimplantation Development

SUMMARY

To elucidate the molecular dynamics of HP1β in mouse preimplantation embryos, I examined the localization, dynamics, and mobility of HP1β in the (pro)nucleus by live-cell imaging. Time-lapse observation revealed that the chromatin association of HP1β is regulated by a cell cycle-dependent manner. HP1β was localized in the interphase nucleus, and dynamically dissociated from the nucleus at the metaphase stage. The HP1β assembly and clustered heterochromatin structure were both found in the nucleus of 2-cell and later stages of embryos. Moreover, fluorescent recovery after photobleaching analysis implied that HP1β is more freely mobile in the pronucleus of 1-cell embryo than in the 4-cell nucleus. These results suggest that the chromatin configuration may be regulated by the stability and mobility of chromatin-associated proteins including HP1β at the early stages of embryo.

INTRODUCTION

Heterochromatin is a specialized chromatin structure containing highly condensed DNA and repressive histone modification, and is implicated in the basic cellular functions such as the dosage compensation of gene expression in X chromosome inactivation (Heard, 2004), repression of inadequate transcription (Lehnertz et al., 2003; Martens et al., 2005), cohesion of kinetochores (Bernard et al., 2001), and stability of chromosomes (Peters et al., 2001). Heterochromatin protein 1, HP1, which interacts with an epigenetic marker, methylated lysine 9 of histone H3, is a component of silent chromatin at telomeres and centromeres (Lachner et al., 2001; Bannister et al., 2001). HP1 is of particular interest, because gene silencing is thought to involve the spreading of heterochromatin proteins in a HP1-dependent manner. Although HP1 has long been believed to bind heterochromatin tightly and stably, fluorescent recovery after photobleaching (FRAP) analysis indicated that HP1 is highly mobile within the heterochromatin and euchromatin (Festenstein et al., 2003; Cheutin et al., 2003). Moreover, the mobility of several chromatin proteins including HP1 and histone dynamically decreases after differentiation of embryonic stem cells into neural progenitor cells (Meshorer et al., 2006).

The nuclear structure including the heterochromatin density and centromere localization is known to be largely different between somatic cells and preimplantation embryos at the early stages (Martin et al., 2006; Yamazaki et al., 2007). Heterochromatin is localized around the nucleolus of pronuclei, whereas embryos after the 4-cell stage contain clustered heterochromatin throughout the nucleus (Martin et al., 2006; Yamazaki et al., 2007). The dynamic conversion of the chromatin structure during

preimplantation development implies a possible involvement of chromatin-associated proteins that may act on the identity establishment of "germ cell" to "embryo." However, little is known of the molecular dynamics of these proteins in preimplantation embryos. In this study, I have thus examined the localization, dynamics, and mobility of mouse HP1β in the (pro)nuclei of early-stage embryos by live-cell imaging analysis.

MATERIALS AND METHODS

Plasmid construction and RNA synthesis *in vitro*

Expression plasmids encoding fusion proteins of enhanced green fluorescence protein (EGFP) or monomeric DsRed (mDsRed, Clontech, Mountain View, CA) with mouse HP1β were prepared as described previously (Yamazaki et al., 2007). Briefly, a cDNA fragment encoding mouse HP1β was PCR-amplified from a first strand mouse brain cDNA library using a set of primers, 5'-CCAAGCTTCATGGGGAAAAAGCAAAACAAG-3' and 5'-AAGCGGCCGCTCAGAATTCATTCTTGTCGTCTTTTTTGTC-3'. The amplified fragment was digested by *Hin*dIII and *Not*I, and introduced to a pcDNA 3.1-polyA vector (Yamagata et al., 2005) together with an *Eco*RI/*Hin*dIII DNA fragment of EGFP or mDsRed at the *Eco*RI and *Not*I sites. Expression plasmids encoding human histone H2B (Kanda et al., 1998) fused to mRFP1 (Campbell et al., 2002) and human CENPB fused to EGFP were constructed as described previously (Yamazaki et al., 2007; Mikami et al., 2005). For RNA synthesis *in vitro*, expression plasmids were linearized by cutting with *Xba*I. RNA with a cap structure at the 5'-end was synthesized by T7 polymerase using a RiboMAX large scale RNA production systems-T7 kit (Promega, Madison, WI), and then by using a Ribo m7G cap analog kit (Promega), according to the manufacture's protocol. The RNA samples were treated with RNase-free DNase I (Promega), extracted with phenol-chloroform, precipitated with ethanol, and purified by gel filtration on MicroSpin G-25 column (GE Healthcare Bio-Sciences, Piscataway, NJ).

Cell culture

NIH3T3 cells were cultured in Dulbecco's modified Eagle's medium (Gibco BRL, Gaithersburg, MD) supplemented with 10% fetal bovine serum, 100 U/ml penicillin, 0.1 mg/ml streptomycin at 37°C under 5% CO_2 in air. The mDsRed-HP1β plasmid was co-transfected with the CENPB-EGFP plasmid into NIH3T3 cells using a PerFectin transfection reagent (Gene Therapy System, San Diego, CA). Cells were further cultured in the same medium for 2 days, and then observed under an Olympus IX-71 fluorescent microscope (Olympus, Tokyo, Japan).

Immunostaining

Cultured cells and embryos were fixed with 4% paraformaldehyde for 60 min, and permeabilized with phosphate-buffered saline (PBS) containing 2% Triton X-100. After blocking with PBS containing 3% normal goat serum and 0.05% Tween-20 for 60 min, cells were incubated with anti-HP1β monoclonal (Chemicon international, Temecula, CA) and anti-histone H2B polyclonal antibodies (Upstate Biotechnology, Lake Placid, NY) for 60 min, washed with PBS, reacted with Alexa Fluor 488 (or 568)-conjugated anti-mouse IgG and Alexa Fluor 568-conjugated anti-rabbit IgG antibodies (Molecular Probes, Eugene, OR), and observed under the above fluorescent microscope.

Gamete collection, RNA microinjection, and insemination

All animal experiments were carried out according to the Guide for the Care and Use of Laboratory Animals in University of Tsukuba. Gamete collection, RNA injection, and insemination were carried out as described previously (Yamazaki et al., 2007). Cumulus-free, metaphase II-arrested eggs from 8- to 12-week-old ICR mice (Japan SLC, Shizuoka, Japan) were

microinjected with synthetic RNA (approximately 2 pl, 50 ng/μl) by a piezo-driven micromanipulator (Prime Tech, Ibaraki, Japan), and incubated at 37°C for 3 h under 5% CO_2 in air. Epididymal sperm heads of ICR mice (3- to 5-month-old) were injected into the eggs, as described previously (Kimura and Yanagimachi, 1995a). The reconstructed embryos were cultured in FHM medium (Lawitts and Biggers, 1993). Cumulus-intact, metaphase II-arrested eggs were also inseminated with capacitated epididymal sperm (50 cells/μl), and incubated for 60 min. The fertilized embryos were then injected with RNA (approximately 2 pl, 5 ng/μl), and incubated with KSOM medium (Lawitts and Biggers, 1993) at 37°C under 5% CO_2 in air. Time-lapse observation of the 1-cell embryos during pronuclear formation and 2-cell cleavage was carried out as described previously (Yamazaki et al., 2007). Only cumulus-free, metaphase II-arrested eggs were inseminated by intracytoplasmic sperm injection (ICSI), owing to a low rate of *in vitro* fertilization (IVF).

Immunoblot analysis

Proteins were separated by SDS-polyacrylamide gel electrophoresis (PAGE), and transferred onto Immobilon-P membranes (Millipore, Bedford, MA). The blots were blocked with 2% skim milk, probed with anti-HP1β or β-tubulin (Sigma, St. Louis, MO) monoclonal antibody for 2 h, and incubated with horseradish peroxidase-conjugated goat anti-mouse IgG + IgM antibody (Jackson Immunoresearch Laboratories, West Grove, PA) for 60 min. After washing, immunoreactive proteins were detected by an ECL plus Western blotting detection kit (GE Healthcare Bio-Sciences), as described previously (Kim et al., 2004).

Fluoromicroscopic analysis

Eggs and embryos were transferred to 20 mM Hepes-buffered TYH (Toyoda et al., 1971) or FHM medium in a 3.5-cm glass-bottomed dishes (Matsunami Glass Industry, Osaka, Japan), and observed under an Olympus IX-71 fluorescent microscope equipped with a CSU-10 Nipkow disk confocal scanning unit (Yokogawa Electric Corp., Tokyo, Japan). Images were captured as vertical sections (approximately 1-5 μm intervals) by an iXon-EMCCD camera (Andor Technology, Belfast, Northern Ireland) using a Z-axis motor. Acquired images were processed by a deconvolution program of a MetaMorph software (Universal Imaging Co., Downingtown, PA), and then stacked into a picture.

FRAP analysis

FRAP analysis were carried out as described previously (Kobayakawa et al., 2007) with some modifications. Briefly, embryos were incubated on a glass-bottomed dish at 37°C under 5% CO_2 in air, treated with the 488 nm line of an argon laser, and observed under a Zeiss LSM 510 confocal microscope (Carl Zeiss, Inc., Jena, Germany). A region of interest (ROI) on the embryo was photobleached with a laser pulse (75% laser power and 100% transmission), and the fluorescent recovery was observed by scanning with a low laser pulse (75% laser power and 5% transmission) at 0.6-s intervals. The fluorescent intensity was measured by using a MetaMorph software. The relative intensity of ROI was determined as $I_{rel}= (T_0\ I_t)/ (I_0\ T_t)$, where T_0, T_t, I_0, and I_t are the total cellular intensity on the pre-bleach image, total cellular intensity at a time point (t), average intensity in the ROI on the pre-bleach image, and average intensity in the ROI at the time point (t), respectively, as described previously (Phair and Misteli, 2000).

RESULTS AND DISCUSSION

I first examined the abundance and localization of EGFP (or mDsRed)-HP1β fusion protein exogenously produced in unfertilized eggs and NIH3T3 cultured cells (Fig. 3). Metaphase II-arrested mouse eggs were microinjected with RNA encoding the EGFP-HP1β protein, incubated for 12 h, and then analyzed by immunoblot analysis using anti-HP1β antibody (Fig. 3A). When the RNA injection was carried out at a concentration of 5 ng/μl, the level of 50-kDa EGFP-HP1β was similar to that of 25-kDa endogenous HP1β in the eggs. Immunostaining of NIH3T3 cells previously transfected with an expression plasmid encoding CENPB-EGFP fusion protein indicated that endogenous HP1β is distributed throughout the cell nucleus, and is enriched in the centromeric region where CENPB-EGFP is present (Fig. 3B). Similar results were obtained by live-cell imaging of NIH3T3 cells co-transfected with the mDsRed-HP1β and CENPB-EGFP plasmids. Since the exogenously expressed HP1β fusion protein behaved similarly to endogenous HP1β in cells, the experimental approach using the EGFP (or mDsRed)-HP1β fusion protein allows us to examine the dynamics of HP1β in living eggs and embryos during preimplantation development.

I next carried out time-lapse observation of EGFP-HP1β in the (pro)nucleus during the transition from 1-cell to 2-cell embryos (Fig. 4). Both EGFP-HP1β and a chromatin marker, H2B-mRFP, were produced in the cytoplasm of metaphase II-arrested eggs by co-injection of the

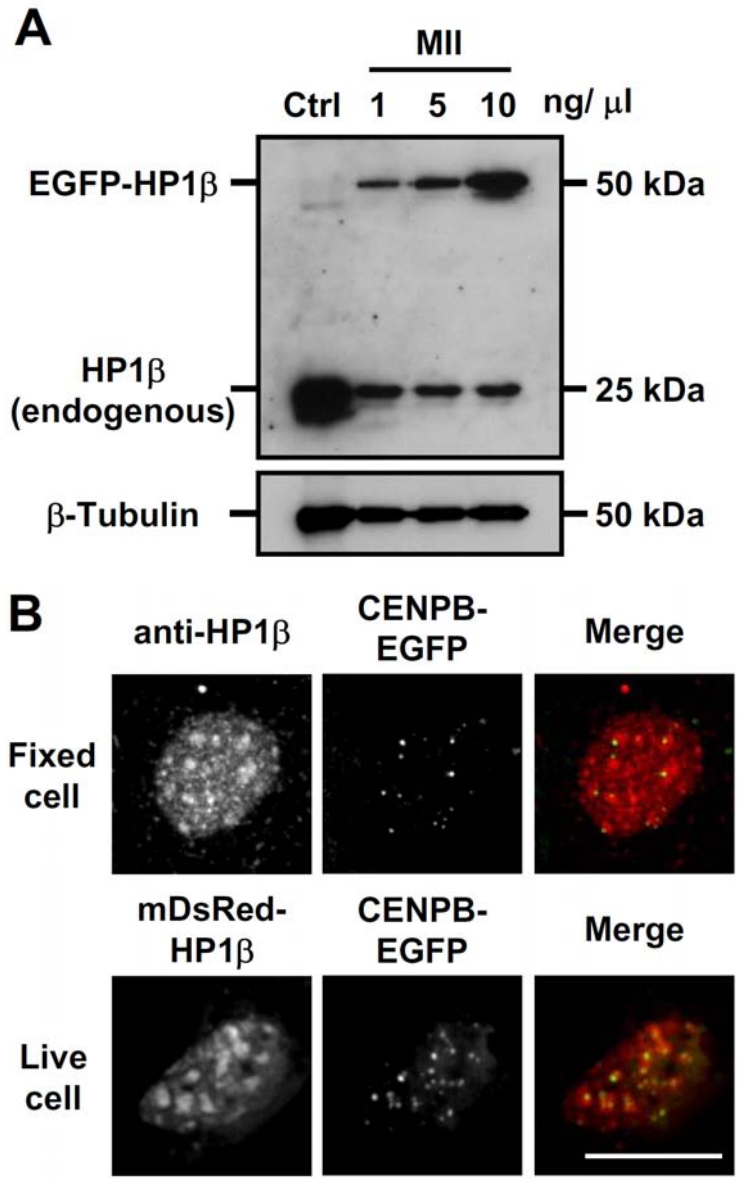

Fig. 3. Validation of exogenously expressed HP1β.
(A) Expression of EGFP-HP1β in metaphase II (MII)-arrested mouse eggs. MII eggs were injected with an *in vitro* synthesized RNA (approximately 2 pl) encoding EGFP-HP1β at 1, 5, and 10 ng/ml, incubated for 12 h, and then subjected to immunoblot analysis (100 eggs/lane). Proteins (10 μg/lane) in testicular extracts were used as a control (Ctrl). (B) Immunostaining of NIH3T3 cultured cells. Endogenously and exogenously expressed HP1β were visualized by immunostaining using anti-HP1β antibody (red) or by live-cell imaging of mDsRed-HP1β fusion protein (red). Centromeres were co-visualized by CENPB-EGFP (green). Scale bar = 10 μm.

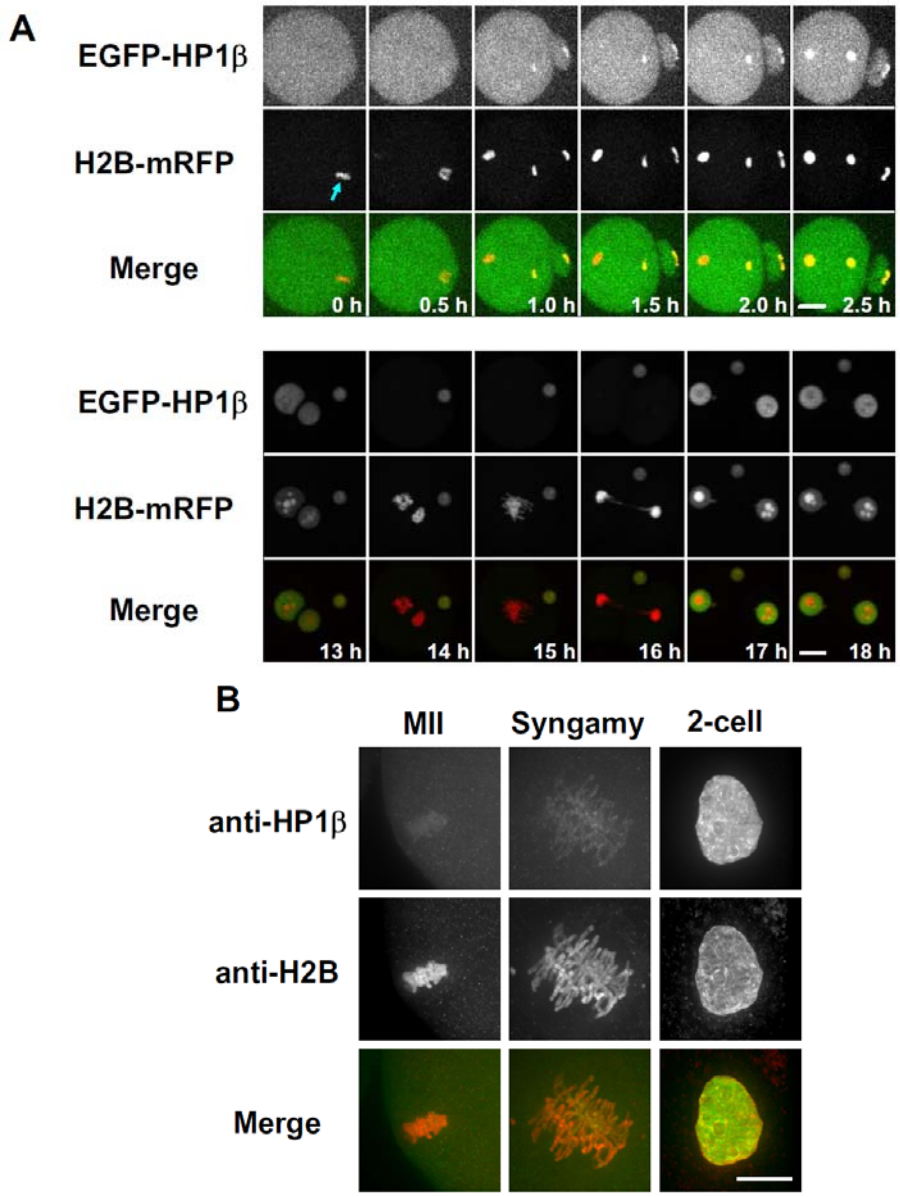

Fig. 4. Time-lapse monitoring of EGFP-HP1β during the transition of 1-cell to 2-cell embryos.

(A) Nuclear dynamics of EGFP-HP1β. Two synthetic RNAs (50 ng/μl each) encoding EGFP-HP1β (green) and H2B-mRFP (red) were co-injected with metaphase II-arrested eggs, and incubated for 3 h *in vitro*. After ICSI, fluorescent images were acquired every 10 min for 22 h. The images at 0- to 2.5-h and 13- to 18-h stages after ICSI are indicated. Enhanced fluorescent images of the EGFP-HP1β-expressing 1-cell embryo at the 0- to 2.5-h stages are shown because EGFP-HP1β is mostly spread throughout the cell cytoplasm. An arrow indicates the female metaphase plate. Scale bar = 20 μm. (B) Immunostaining analysis. Metaphase II (MII)-arrested eggs, metaphase-stage 1-cell embryos (syngamy), and 2-cell embryos were subjected to immunostaining using anti-HP1β (green) and anti-H2B (red) antibodies. Scale bar = 10 μm.

corresponding RNAs approximately 3 h after the injection (data not shown). The female chromosome was distinguished from the male chromosome by the presence of H2B-mRFP in the metaphase plate soon after ICSI (arrow in Fig. 4A). EGFP-HP1β was still present in the cytoplasm 0.5 h after ICSI, and was then co-localized with H2B-mRFP only in the female chromosome until 2.5 h after ICSI (Fig. 4A). In the male pronucleus, H2B-mRFP was initially recruited to the chromosome around 1 h after ICSI. EGFP-HP1β was absent at 1-, 1.5-, and 2-h stages after ICSI, and was partially recruited into the pronucleus at the 2.5-h stage. EGFP-HP1β was then dissociated from the male and female pronuclei, re-distributed in the cytoplasm at the metaphase stage 14-16 h after ICSI, and translocated into the nucleus of the 2-cell embryo at the 17- and 18-h stages. Interestingly, H2B-mRFP and EGFP-HP1β were predominantly present in the nucleolus and nucleoplasm of the 2-cell nucleus, respectively. Immunostaining analysis using anti-HP1β and anti-H2B antibodies verified the absence of HP1β from the chromosomes of metaphase II-arrested egg and mitotic 1-cell embryo (Fig. 4B). It has been previously demonstrated that the α-, β-, and γ-forms of HP1 bind to the tri-methylated lysine 9 residue of histone H3, and dissociate from the chromosome when the serine residue of histone H3 at position 10 is phosphorylated by Aurora B kinase during mitosis of cultured cells (Fischle et al., 2005; Hirota et al., 2005). Thus, our data suggest that the binding/dissociation interaction of HP1β with the chromatin in the transition of 1-cell to 2-cell embryos may be regulated by the similar mechanism in cultured cells.

To examine the conformational dynamics of heterochromatin during preimplantation development, EGFP-HP1β fluorescence in the nucleus of

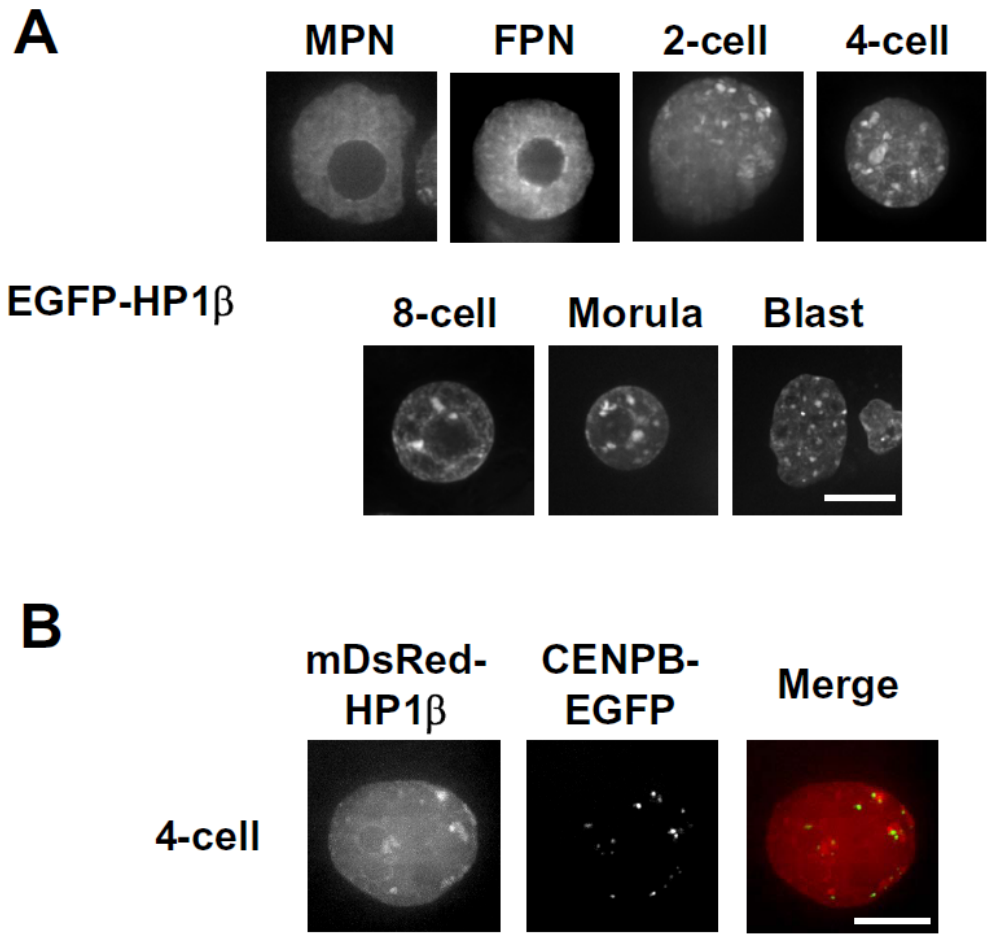

Fig. 5. Live-cell imaging analysis of preimplantation embryos.
(A) Dynamic change of EGFP-HP1β localization during preimplantation development. Metaphase II-arrested eggs were inseminated with epididymal sperm and incubated for 2-3 h after insemination. Synthetic RNA (5 ng/μl) encoding EGFP-HP1β was injected into the fertilized embryos. The embryos at the 1-cell, 2-cell, 4-cell, 8-cell, morula, and blastocyst (Blast) stages were prepared 12, 24, 48, 60, 72, and 96 h after insemination, respectively. Scale bar = 10 μm. MPN, male pronucleus; FPN, female pronucleus. (B) Localization of mDsRed-HP1β and CENPB-EGFP in 4-cell embryos. Fertilized embryos were co-injected with synthetic RNAs (50 ng/μl each) encoding mDsRed-HP1β (red) and CENPB-EGFP (green), and incubated for 48 h after insemination. Scale bar = 10 μm.

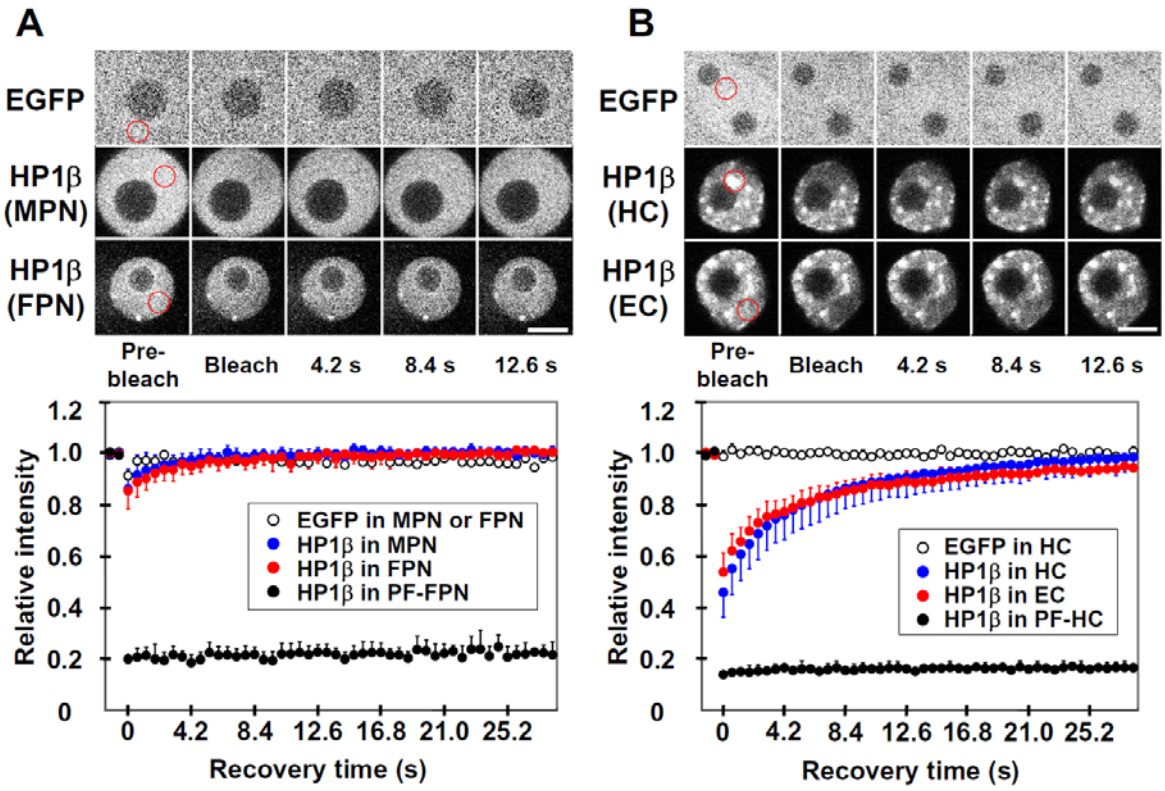

Fig. 6. Mobility of EGFP-HP1β in the (pro)nuclei of 1-cell and 4-cell embryos.
(A) Fluorescent recovery of EGFP and EGFP-HP1β in 1-cell embryos. Synthetic RNA (5 ng/ml) encoding EGFP or EGFP-HP1β was injected into the fertilized embryos 60 min after insemination, incubated for 10-12 h, and subjected to FRAP analysis. Regions of interests (red circles) on the male (MPN) and female (FPN) pronuclei were photobleached. The fluorescent recovery after photobleaching was quantitatively analyzed using 4 EGFP-expressing, 10 EGFP-HP1β-expressing (for MPN), 7 EGFP-HP1β-expressing (for FPN), and 5 EGFP-HP1β-expressing and 4% paraformaldehyde-fixed (PF) 1-cell embryos, respectively. The data are indicated as mean ± SD. Scale bar = 10 μm. (B) Fluorescent recovery of EGFP and EGFP-HP1β in 4-cell embryos. The EGFP-HP1β-assembled and non-assembled regions (red circles) probably corresponding to heterochromatin (HC) and euchromatin (EC), respectively, were photobleached. The fluorescent recovery after photobleaching was quantitatively analyzed using 4 EGFP-expressing, 14 EGFP-HP1β-expressing (for HC), 12 EGFP-HP1β-expressing (for EC), and 4 EGFP-HP1β-expressing and 4% paraformaldehyde-fixed (PF) 4-cell embryos, respectively. The data are indicated as described above. Scale bar = 10 μm.

fertilized embryo previously injected with the corresponding RNA was monitored by live-cell imaging (Fig. 5A). The fluorescence was uniformly distributed throughout the nucleoplasm of the male and female pronuclei, without a clear cluster assembly. The nucleus of 2-cell embryo contained small dotted signals that were still dispersed throughout the nucleus. In 4-cell, 8-cell, and morula embryos, the fluorescent signals were assembled to form the large dots in the nucleus. Moreover, the size of the nuclear fluorescent dots in blastocysts was smaller than that in morula. When 4-cell embryos previously co-injected with mDsRed-HP1β and CENPB-EGFP RNAs were observed by live-cell imaging, the CENPB-EGFP signals were largely overlapping with the mDsRed-HP1β signals assembled in the nucleus (Fig. 5B). These data suggest that the cluster structure of heterochromatin may begin to be formed at the 2-cell stage, and may be co-localized with the centromeric chromatin.

As shown in Fig. 6, FRAP analysis was carried out to examine the mobility of EGFP-HP1β in the (pro)nuclei of 1-cell and 4-cell embryos. The fluorescence in the EGFP-expressing 1-cell (Fig. 6A) and 4-cell embryos (Fig. 6B) recovered within the bleached region immediately after the bleaching episode, whereas there was no recovery of fluorescence in the EGFP-HP1β-expressing 1-cell and 4-cell embryos fixed with 4% paraformaldehyde. The EGFP-HP1β fluorescence in the bleached regions of the male and female pronuclei of 1-cell embryo restored within approximately 4 s, implying that HP1β is very freely mobile in the pronuclei of living 1-cell embryo. No significant difference of the fluorescence recovery was found between the male and female pronuclei. In the EGFP-HP1β-expressing 4-cell embryos, the region forming the cluster assembly of EGFP-HP1β probably corresponding to the heterochromatin region quickly restored the

EGFP-HP1β fluorescence by approximately 10 s after the end of the bleaching episode, and then gradually returned to the normal level observed prior to bleaching within 25 s. The time course of the EGFP-HP1β fluorescent intensity in the diffused region corresponding to euchromatin showed the similar recovery in the bleached region. These data suggest that chromatin may gradually turn to a stable structure during early embryogenesis, because EGFP-HP1β is exchanged on the binding sites at faster rate in the 1-cell pronucleus than in the 4-cell nucleus.

This study indicates that the chromatin configuration and mobility of HP1β in the nucleus are both dynamic and changeable during preimplantation development. Our data also suggest that the level of chromatin-associated HP1β may be low in the pronuclei of 1-cell embryo, because no significant difference of the HP1β mobility is found between the EGFP- and EGFP-HP1β-expressing 1-cell embryos (Fig. 6). It is thus possible that the stability and mobility of chromatin-associated proteins including HP1β regulate the chromatin configuration at the early stages of embryo.

CHAPTER II

Time-lapse and Retrospective Analysis of DNA Methylation in Mouse Preimplantation Embryos by Live-cell Imaging

SUMMARY

Genome-wide change of DNA methylation in preimplantation embryos is known to be important for the nuclear reprogramming process. A synthetic RNA encoding enhanced green fluorescence protein fused to the methyl-CpG-binding domain and nuclear localization signal of human MBD1 was microinjected into metaphase II-arrested or fertilized embryos, and the localization of methylated DNA was monitored by live-cell imaging. Both the central part of decondensing sperm nucleus and the rim region of the nucleolus in the male pronucleus were highly DNA methylated during pronuclear formation. The methylated paternal genome undergoing active DNA demethylation in the enlarging pronucleus was dispersed, assembled, and then migrated to the nucleolar rim. The female pronucleus contained methylated DNA predominantly in the nucleoplasm. When the localization of methylated DNA in preimplantation embryos was examined, a configurational change of methylated chromatin dramatically occurred during the transition of 2-cell to 4-cell embryos. Moreover, retrospective analysis demonstrated that a noticeable number of the embryos reconstructed by round spermatid injection (ROSI) possess small, bright dots of methylated chromatin in the nucleoplasm of male pronucleus. These ROSI embryos showed a significantly low rate of 2-cell formation, thus suggesting that the poor embryonic development of the ROSI embryos may result from the abnormal localization of methylated chromatin.

INTRODUCTION

Methylation of the cytosine residue in CpG dinucleotide plays a crucial role in the regulation of gene suppression such as X-chromosome inactivation, genomic imprinting, and inactivation of transposable elements (Ferguson-Smith and Surani, 2001; Jones and Takai, 2001; Jones et al., 1998; Li, 2002). The genome-wide change of DNA methylation is also implicated in the nuclear reprogramming during preimplantation development (Fulka et al., 2004; Reik et al., 2001). Following fertilization, methylated zygotic genomes undergo globally active and passive DNA demethylation in preimplantation development, and then the parental genomes acquire new methylation patterns specific for the cell types after the implantation of embryos. Embryos, which have been reconstructed by nuclear transfer of somatic cells, occasionally exhibit an aberrant pattern of DNA methylation at the preimplantation stages (Beaujean et al., 2004; Dean et al., 2001; Kang et al., 2001). In addition, embryos cultured under unusual conditions result in the developmental failure because of the disordered methylation pattern (Shi and Haaf, 2002). Thus, the precise regulation of DNA methylation in the preimplantation embryos is essential for the normal development.

Indirect immunostaining using anti-5-methylcytosine (5mC) antibody is usually utilized to examine the state of DNA methylation in fertilized embryos and early embryos. However, there are several disadvantages for the use of the antibody. The intact chromatin structure is probably destroyed by an HCl treatment required for enhancement of the antibody accessibility to methylated DNA (Jorgensen et al., 2006). It is also difficult to observe living cells in real time due to the cell fixation. I (Yamagata et al., 2005) have recently established a monitoring system that allows visualization of

methylated DNA in living eggs and embryos previously microinjected with a synthetic RNA encoding enhanced green fluorescence protein (EGFP) fused to the methyl CpG binding domain (MBD) and nuclear localization signal (NLS) of human methyl CpG binding protein 1 (MBD1) (Fujita et al., 1999).

In this study, I have carried out time-lapse and retrospective analysis of DNA methylation in living mouse preimplantation embryos, using the above monitoring system. Time-lapse recording provides several new insights into the methylated chromatin dynamics in the (pro)nuclei of fertilized embryos and early embryos: the migration and rearrangement of DNA-methylated sperm genome during pronuclear formation, the localization of methylated DNA in the male and female pronuclei, and the reconstitution of methylated chromatin during preimplantation development. Moreover, the comparison of DNA methylation states between the embryos reconstructed by intracytoplasmic sperm injection (ICSI) and round spermatid injection (ROSI) shows the abnormal localization of methylated chromatin only in the male pronuclear nucleoplasm of the ROSI embryos. This abnormality may explain the reason for a low rate of successful embryogenesis after ROSI.

MATERIALS AND METHODS

Plasmid construction

Expression plasmids encoding fusion proteins of EGFP or monomeric DsRed (mRFP, Clontech, Mountain View, CA) with MBD and NLS of human MBD1, and of EGFP with human centromeric protein B (CENPB) were constructed as described (Shelby et al., 1996; Yamagata et al., 2005). Briefly, DNA fragments encoding MBD, NLS, and CENPB were PCR-amplified from a first-strand cDNA library of HeLa cells using following primer sets: 5'-CCAAGCTTCATGGCTGAGGACTGGCTGGAC-3' and 5'-AAGCGGCCGCTTACGGGGCCTCCTTCCTGACCT-3' for MBD; 5'-CCAAGCTTCTGCTATCCAGCCCCCAAGGC-3' and 5'-AAGCGGCCGCTTACGGGGCCTCCTTCCTGACCT-3' for NLS; 5'-AGAATTCGCCACCATGGGCCCCAAGAGGCGACAG-3', and 5'-GGAAGCTTGAGCTCGAGATCAGTGCTCCCGCCACTGCCCT-3' for CENPB. The amplified fragments were digested by appropriate restriction enzymes, and ligated to a pcDNA 3.1-polyA vector (Yamagata et al., 2005) together with a DNA fragment of EGFP or mRFP. Two MBD mutants (Fujita et al., 2000), R30A and D32A, containing Ala residues instead of Arg and Asp at positions 30 and 32 in MBD, were prepared by site-direct mutagenesis using the following primer sets: 5'-CCACCTGTGGAGCCTCAGACACCTATTAC-3' and 5'-GTAATAGGTGTCTGAGGCTCCACAGGTGG-3' for R30A, and 5'-GGACGCTCAGCCACCTATTACC-3' and 5'-GGTAATAGGTGGCTGAGCGTCC-3' for D32A. For expression of EGFP-MBD-NLS plasmids in *Escherichia coli*, the MBD fragments were amplified by using 5'-CCAAGCTTCATGGCTGAGGACTGGCTGGAC-3'

and 5'-AAGCGGCCGCCGGGGCCTCCTTCCT-3', digested by restriction enzymes, and then introduced into a pET23d (Novagen, Madison, WI) vector with a fragment of EGFP from pEGFP-C2 (Clontech, Mountain View, CA). The plasmids were expressed in *E. coli* BL21 (DE3), and recombinant proteins produced were purified by using an Ni-NTA His Bind resin (Novagen, Madison, WI). Expression plasmids encoding 386- and 42-residue *Spiroplasma monobiae* CpG methyltransferase SssI fused to the gal4 binding domain (GAL4BD) at the N-terminus were prepared as described (Yamagata et al., 2005). GAL4BD was used for the transport of SssI to the cell nucleus.

Dot blot assays

A CpG-methylated DNA was prepared by treatment of pUC19 with SssI methyltransferase (New England Biolabs, Ipswich, MA) according to the manufacture's instruction. The methylated plasmid was recovered using a Wizard DNA Clean-up kit (Promega, Madison, WI), extracted with phenol-chloroform, and precipitated by ethanol. The methylated pUC19 DNA was spotted on Hybond-N^+ nylon membrane (GE Healthcare Bio-Sciences Corp., Piscataway, NJ), fixed with 0.4 M NaOH, washed, blocked with 5% skim milk, mixed with recombinant proteins (8 μg/ml) or anti-5mC antibody (Eurogentec, Seraing, Belgium, catalogue number MMS-900P-A), and incubated for 60 min at room temperature in phosphate-buffered saline (PBS). Fluorescence was measured by a Molecular Imager FX fluorescence scanner (Bio-Rad Laboratories, Hercules, CA,).

Cell culture

NIH3T3 cells were cultured in Dulbecco's modified essential medium (Gibco BRL, Gaithersburg, MD) supplemented with 10% fetal bovine serum, 100 U/ml penicillin, 0.1 mg/ml streptomycin, and 0.5 μM DNA methyltransferase inhibitor 5-aza-2'-deoxycytidine (5-AzaC, ICN Biomedicals, Inc., Costa Mesa, CA) at 37°C under 5% CO_2 in air for 4 days. EGFP-MBD-NLS plasmid was co-transfected with mRFP-NLS plasmid into 5-AzaC-treated NIH3T3 cells, using a PerFectin transfection reagent (Gene Therapy System, San Diego, CA). Cells were further cultured in the above medium for 2 days, and then observed under an Olympus IX-70 fluorescent microscope (Tokyo, Japan).

Immunostaining

Cultured cells were fixed with 4% paraformaldehyde for 60 min, permeabilized with PBS containing 2% Triton X-100 for 30 min, treated with 2 M HCl for 30 min, and washed thoroughly with 0.1 M Tris/HCl, pH 8.0. After blocking in PBS containing 3% normal goat serum, cells were incubated with anti-5mC and anti-histone H2B antibodies (Upstate Biotechnology, Lake Placid, NY, catalogue number 07-371), reacted with Alexa 488-conjugated anti-mouse IgG and Alexa 568-conjugated anti-rabbit IgG antibody (Molecular Probes, Eugene, OR, catalogue numbers A11029 and A11036, respectively), counterstained with propidium iodide (3 μg/ml), and observed under the above fluorescent microscope. Embryos were immunostained as described above, except for the time of HCl treatment (10 min).

Gamete collection, RNA microinjection, and insemination

All animal experiments were carried out according to the Guide for the Care and Use of Laboratory Animals in University of Tsukuba. Gamete

collection, RNA injection, and insemination were carried out as described (Yamagata et al., 2005). Metaphase II-arrested eggs from 8- to 12-week-old ICR mice (Japan SLC, Shizuoka, Japan) were injected with RNA (5 or 10 ng/μl) by a piezo-driven micromanipulator (Prime Tech, Ibaraki, Japan). After incubation at 37°C for 3 h under 5% CO_2 in air, the eggs were inseminated in TYH medium (Toyoda, 1971) with capacitated sperm (200 cells/μl) from ICR mice. Cumulus-intact, metaphase II-arrested eggs were inseminated with capacitated sperm (50 cells/μl), and incubated for 60 min. The fertilized embryos were recovered, injected with RNA (5 ng/μl), and then incubated at 37°C under 5% CO_2 in air.

ROSI and ICSI

Metaphase II-arrested eggs, cauda epididymal sperm, and round spermatids in seminiferous tubules were obtained from B6D2F1 mice (8-12 weeks old, Japan SLC). ROSI and ICSI were carried out by the already established methods (Kimura and Yanagimachi, 1995a; Kimura and Yanagimachi, 1995b). Briefly, round spermatids were suspended in PBS containing 5.6 mM glucose, 5.4 mM sodium lactate, 0.01% polyvinylpyrrolidone, and bovine serum albumin (5 mg/ml). The embryos injected with round spermatids were artificially activated by Ca^{2+}-free CZB medium (Chatot et al., 1989) containing 5 mM $SrCl_2$ 40 min before ROSI. ICSI was carried out by injection of epididymal sperm heads into the eggs. The reconstructed embryos were cultured in KSOM medium (Lawitts and Biggers, 1993).

Fluoromicroscopic analysis

Eggs and embryos were transferred to 20 mM Hepes-buffered TYH

(Toyoda, 1971) or FHM (Lawitts and Biggers, 1993) medium in a 3.5-cm glass-bottomed dishes (Matsunami Glass Industry, Osaka, Japan), and observed under the above fluorescent microscope equipped with an incubator box. Images were captured as vertical sections (approximately 1-5 μm intervals) using a Z-axis motor, processed by a deconvolution program of a MetaMorph software (Universal Imaging Co., Downingtown, PA), and then stacked into one picture. The pictures acquired were pseudo-colored using the MetaMorph software. The intensity of fluorescence was measured by using an ImageJ software (http://rsb.info.nih.gov/ij/).

RESULTS

Specific binding of EGFP-MBD-NLS fusion protein to methylated DNA

To ascertain whether EGFP-MBD-NLS fusion protein specifically binds the methylated cytosine residue of CpG dinucleotide, recombinant proteins, including two mutant proteins lacking functional MBD, EGFP-R30A-NLS and EGFP-D32A-NLS, were produced in *E. coli* (Fig. 7A). Binding assays indicated that the EGFP-MBD-NLS protein as well as anti-5mC antibody is capable of binding methylated pUC19 DNA in a dose-dependent manner (Fig. 7B). No significant binding of EGFP-R30A-NLS and EGFP-D32A-NLS to the methylated DNA was found (up to 0.4 μg DNA). When metaphase II-arrested eggs were injected with RNA encoding each of four EGFP fusion proteins before insemination *in vitro*, EGFP-MBD-NLS was distinguished from three other proteins by the shapes of fluorescent signals in the male and female pronuclei (Fig. 7C). The EGFP-MBD-NLS signals were observed as small focal dots in the male nucleolus and female nucleoplasm and nucleolus, whereas three other proteins gave only very smooth signals throughout the male and female pronuclei. The co-injection of EGFP-MBD-NLS RNA with an excess amount of methylated or unmethylated pUC19 (250 ng/μl) into the cytoplasm of fertilized embryos revealed the difference of the subcellular localization of the EGFP fluorescence in cells; the fluorescence was predominantly present in the cytoplasm and nucleus of the pronuclear-stage embryos previously injected with methylated and unmethylated pUC19, respectively (Fig. 8A). When EGFP-MBD-NLS RNA was co-injected with RNA encoding 386-residue (enzymatically active) or 42-residue (inactive) CpG methyltransferase SssI fused to GAL4BD into fertilized embryos, the intensity of EGFP fluorescence

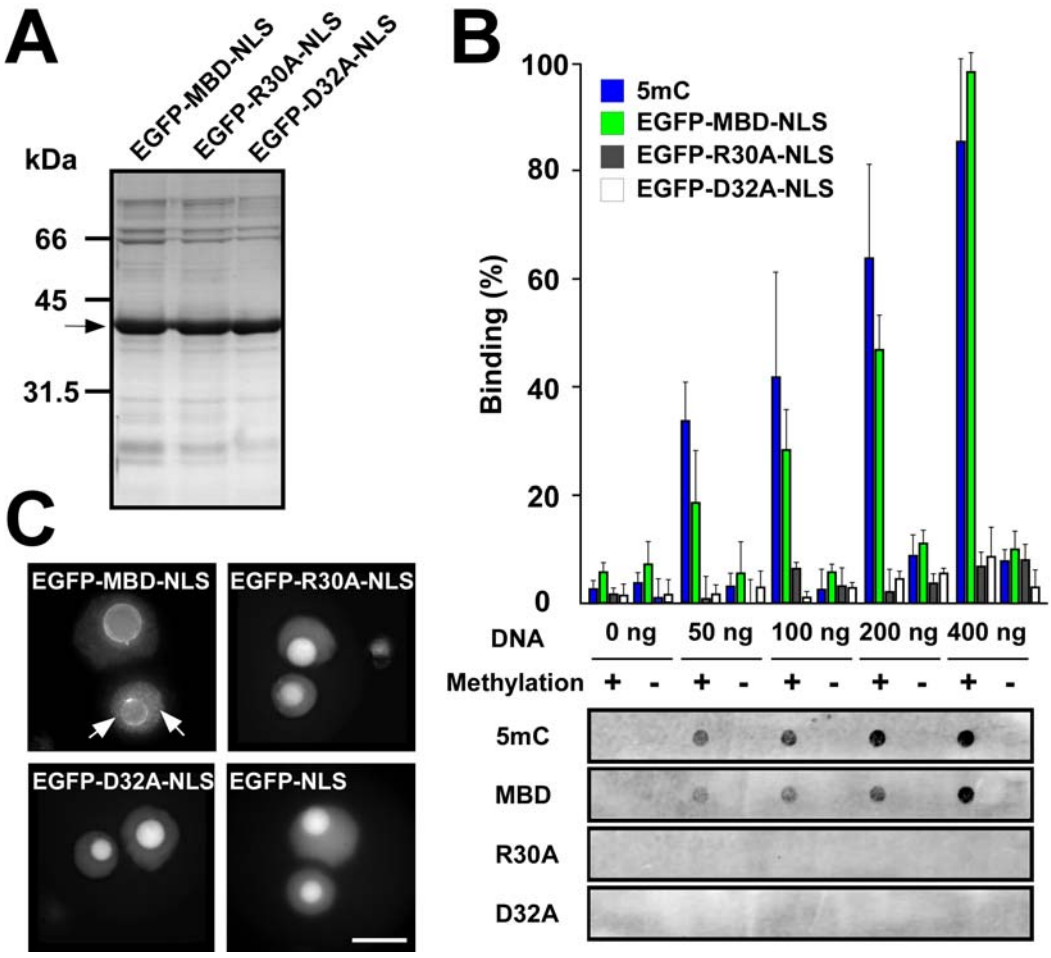

Fig. 7. Binding activity of EGFP-MBD-NLS fusion proteins to methylated DNA.

(A) Production of recombinant fusion proteins. His-tagged recombinant proteins of EGFP-MBD-NLS, EGFP-R30A-NLS, and EGFP-D32A-NLS (arrow) were produced in *E. coli*, and purified by using Ni-NTA His Bind resin. After SDS-PAGE, proteins on gels were stained with Coomassie brilliant blue. (B) Binding of EGFP-MBD-NLS to methylated pUC19 DNA *in vitro*. The CpG-methylated pUC19 was prepared by treatment with SssI methyltransferase. The methylated (+) and unmethylated (-) DNAs (0-0.4 mg) were spotted onto Hybond-N+ nylon membranes, incubated with recombinant proteins (8 μg/ml) or anti-5mC antibody (5mC), washed, and observed by a fluorescence scanner. Data are expressed as the means ± S.E., where n = 3. (C) Localization of EGFP-MBD-NLS fluorescence in pronuclear-stage embryos. Metaphase II-arrested eggs were injected with RNA encoding each of four EGFP fusion proteins (16, 16, 14, and 10 embryos for EGFP-MBD-NLS, EGFP-R30A-NLS, EGFP-D32A-NLS, and EGFP-NLS, respectively), inseminated, incubated for 15 h, and observed under a fluorescent microscope. Dotted signals (arrows) are present only in the EGFP-MBD-NLS-expressing female pronucleus. Scale bar, 20 μm.

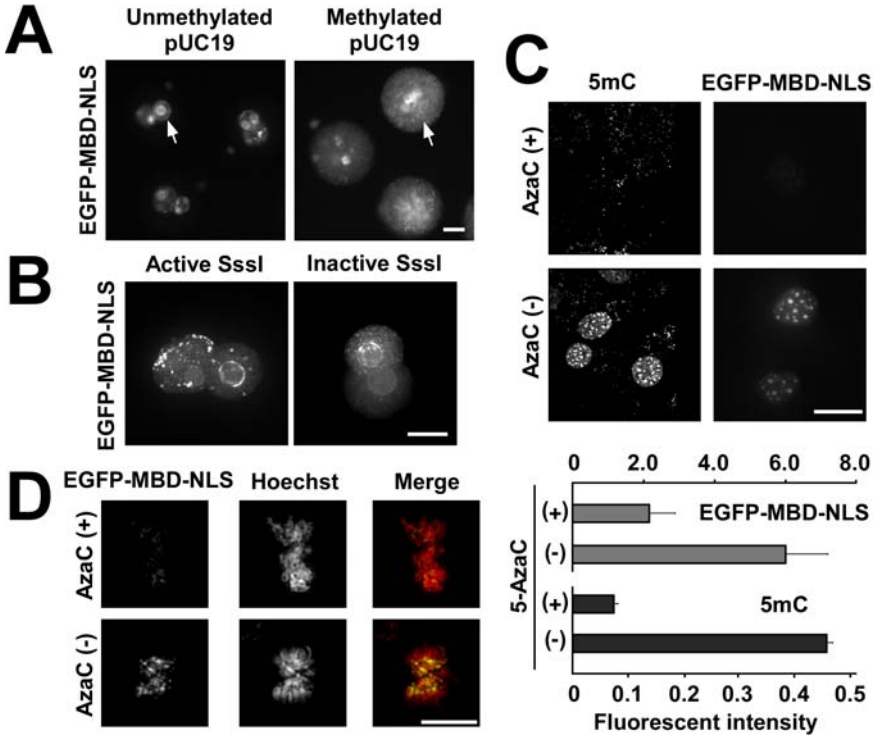

Fig. 8. Specific binding of EGFP-MBD-NLS fusion protein to methylated DNA *in vivo*.

(A) Binding of EGFP-MBD-NLS to methylated pUC19 DNA *in vivo*. EGFP-MBD-NLS RNA was co-injected with methylated and unmethylated pUC19 (250 ng/μl) into the cytoplasm of fertilized embryos (34 and 30 cells, respectively), incubated for 12 h, and observed. Arrows indicate the localization of EGFP-MBD-NLS in the nucleus (left panel) or cytoplasm (right panel) of the embryos. (B) Fluorescent patterns of EGFP-MBD-NLS in pronuclei of fertilized embryos containing enzymatically active or inactive CpG methyltransferase SssI. EGFP-MBD-NLS RNA was co-injected into fertilized embryos (51 and 32 embryos) with RNA encoding 386-residue (active) and 42-residue (inactive) SssI fused to GAL4BD, respectively. The male and female pronuclei were observed 12-15 h after insemination. Scale bar, 20 μm. (C) Fluorescent patterns of NIH3T3 cells treated with DNA methylation inhibitor 5-AzaC. Cells were co-transfected with EGFP-MBD-NLS and mRFP-NLS plasmid DNAs, cultured in the presence (+) and absence (-) of 5-AzaC (AzaC), and observed under a fluorescent microscope. Untransfected cells were co-probed with anti-5mC (5mC) and anti-histone H2B antibodies. The EGFP fluorescence of 14 and 15 cells treated with and without 5-AzaC was measured (20 and 25 cells for anti-5mC antibody), respectively. The fluorescent intensities of the signals detected by anti-5mC antibody and EGFP-MBD-NLS were normalized to those by anti-histone H2B antibody and mRFP-NLS, respectively. Scale bar, 20 μm. (D) Fluorescent patterns of EGFP-MBD-NLS at the metaphase stage of NIH3T3 cells treated with 5-AzaC. Cells expressing EGFP-MBD-NLS were cultured in the presence (+) and absence (-) of 5-AzaC. Following counterstaining with Hoechst 33342 (Hoechst), 24 and 10 cells treated with and without 5-AzaC, respectively, were observed. The images merged are represented as green and red colors for EGFP-MBD-NLS and Hoechst, respectively. Scale bar, 20 μm.

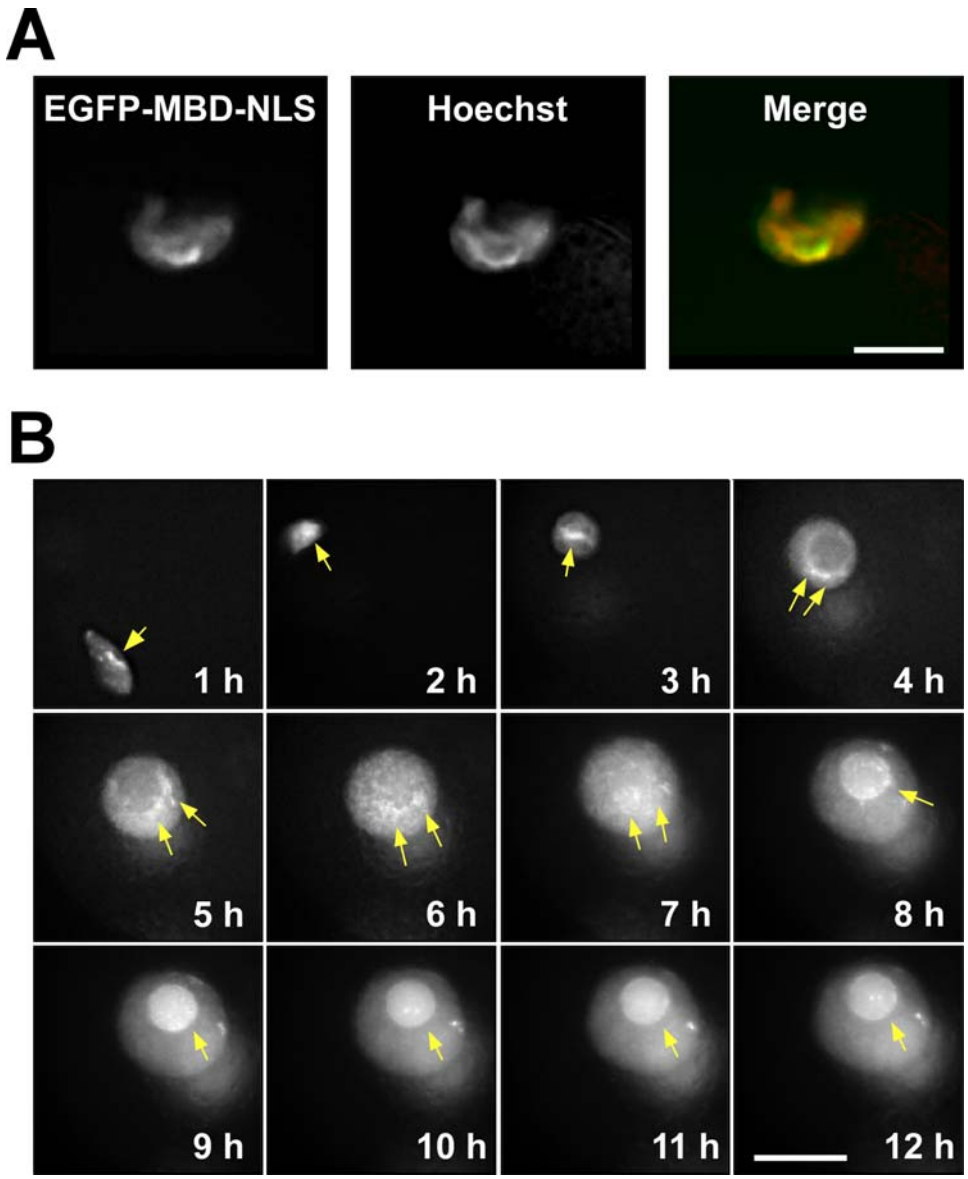

Fig. 9. Time-lapse monitoring of methylated DNA during male pronuclear formation. (A) Patterns of EGFP-MBD-NLS and Hoechst 33342 fluorescence in the decondensing sperm nucleus. EGFP-MBD-NLS RNA was injected into metaphase II-arrested eggs, incubated for 3 h, and inseminated. The embryos were recovered 60 min after insemination, washed, counterstained with Hoechst 33342 (Hoechst), and monitored under a fluorescent microscope. The nuclei of 7 different sperm were observed. The images merged are represented as green and red colors for EGFP-MBD-NLS and Hoechst, respectively. Scale bar, 10 μm. (B) Migration of methylated paternal genome to the nucleolar rim of male pronucleus. The fluorescent images of 29 different pronuclei were acquired every 60 min after insemination. Arrows indicate highly methylated regions in the male pronucleus. Scale bar, 20 μm.

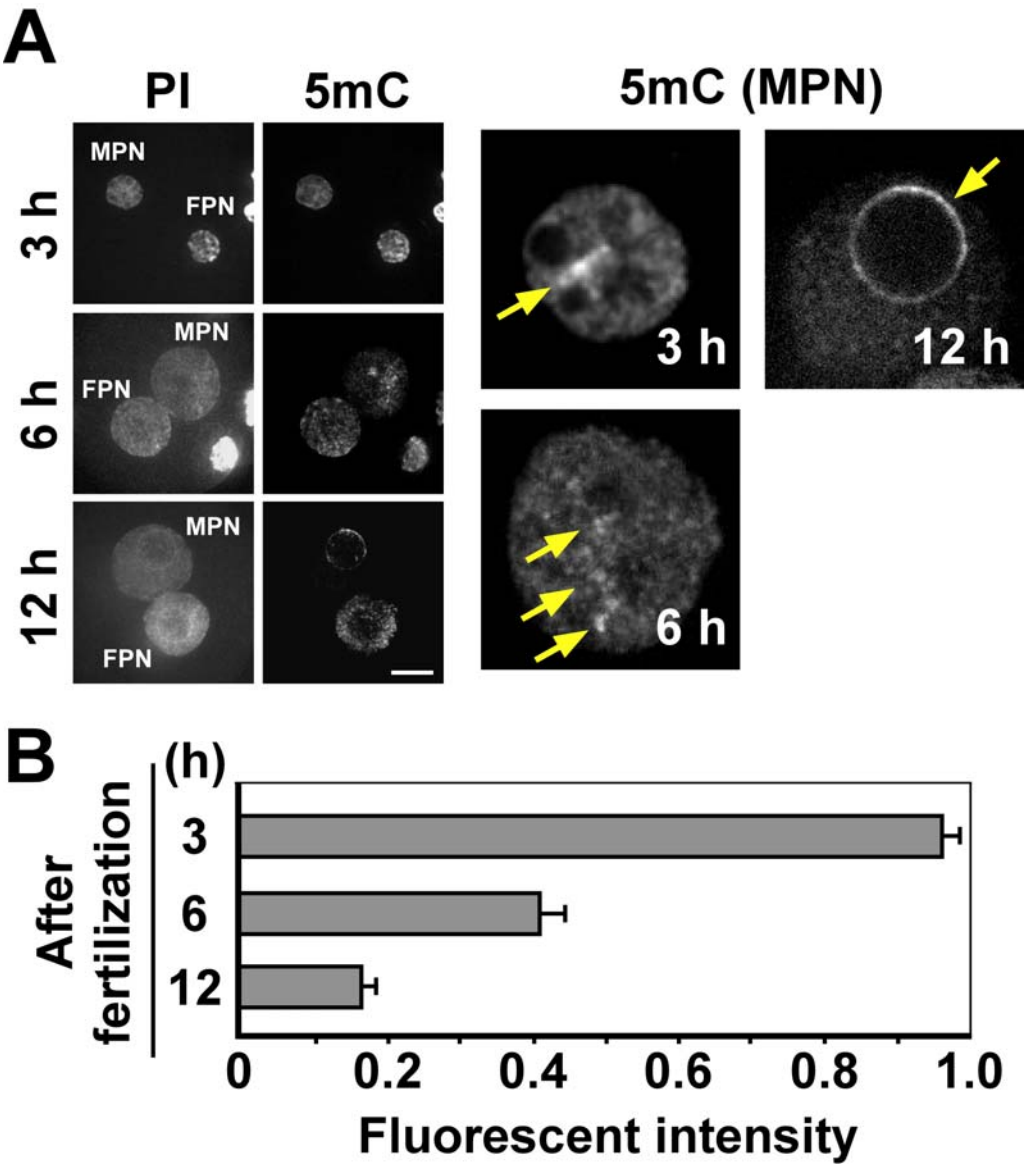

Fig. 10. Validation of time-lapse monitored patterns of methylated DNA localization during male pronuclear formation by immunostaining.

(A) Immunostaining of pronuclear-stage embryos using anti-5mC antibody. The fertilized embryos (11, 12, and 10 cells at 3, 6, 12 h after insemination, respectively) were fixed, treated with HCl, immunostained with anti-5mC antibody (5mC), counterstained with propidium iodide (PI), and then observed under a fluorescent microscope. Enlarged images are also indicated. MPN, male pronucleus; FPN, female pronucleus; PB, polar body. Scale bar, 20 μm. (B) DNA demethylation during male pronuclear enlargement. The intensity of the 5mC fluorescence in the male pronucleus was normalized by those of the PI fluorescence in the male pronucleus, and of the 5mC fluorescence in the female pronucleus within the same embryo. Data are indicated as means ± S.E.

as dotted signals remarkably increased in the pronuclei of the embryos expressing GAL4BD-active SssI (Fig. 8B). Moreover, NIH3T3 cells treated with 5-AzaC, a DNA methyltransferase inhibitor, exhibited a striking decrease in the fluorescent intensity of the interphase nuclei when cells were probed by EGFP-MBD-NLS and anti-5mC antibody (Fig. 8C). In the metaphase chromosome, the dotted signals of EGFP-MBD-NLS were localized in the heterochromatin stained with Hoechst 33342 (Fig. 8D), consistent with the patterns of metaphase-stage germ and Sertoli cells stained with anti-5mC antibody (Bernardino-Sgherri et al., 2002). These data verify the specific binding of EGFP-MBD-NLS to methylated DNA.

Assembly of highly methylated region in male chromatin to nucleolar rim

I next carried out time-lapse observation of methylated DNA in the male nucleus during pronuclear formation. Prior to insemination, EGFP-MBD-NLS was produced in metaphase II-arrested eggs by injection of the corresponding RNA. The fluorescence of EGFP-MBD-NLS overlapping with that of Hoechst 33342 capable of staining the pericentric heterochromatin (Schaufele et al., 2001) was found intensely in the central part of decondensing sperm nucleus immediately after fusion between sperm and egg (60 min after insemination, see Fig. 9A). The intensely fluorescent signal was retained in the enlarging male pronucleus until 3-4 h after insemination, dispersed throughout the pronucleus at the 5- and 6-h stages, assembled at the 7-h stage, and then moved to the rim of the nucleolus (Fig. 9B).

To ascertain whether the fluorescent signals in the male pronucleus indeed reflect the specific binding of EGFP-MBD-NLS to methylated DNA, I carried out immunostaining of fertilized embryos 3, 6, and 12 h after

insemination, using anti-5mC antibody (Fig. 10A). Subsequent quantitative analysis was also carried out (Fig. 10B) because the RNA-injection method employed was inadequate to quantify the level of DNA methylation. The immunostained signals in the male pronucleus were found in the nucleoplasm and nucleolar rim at the 6-h and 12-h stages, respectively. The levels of DNA methylation in the male pronucleus at the 6-h and 12-h stages were approximately 40 and 20% of that at the 3-h stage, respectively (Fig. 10B). In addition, the female pronucleus contained the signals mostly in the nucleoplasm at the 6-h and 12-h stages (Fig. 10A). Although the fluorescence quantification employed in the present study is semi-quantitative, these results are consistent with the fact that the paternal genome undergoes active DNA demethylation during pronuclear enlargement (Mayer et al., 2000; Santos et al., 2002 and 2005). Therefore, the dynamic movement of the methylated chromatin, together with DNA demethylation, occurs in the male pronucleus. It should be noted that the highly methylated region is still present around the rim of the male nucleolus even 12 h after insemination (Fig. 9B and Fig. 10A), supporting the probability that the centromeric region is resistant to DNA demethylation (Santos et al., 2005).

Pericentric region is highly DNA-methylated during preimplantation development

To examine the precise localization of methylated DNA in preimplantation embryos, the fluorescence in the nuclei of fertilized embryos previously injected with EGFP-MBD-NLS RNA were monitored by live-cell imaging (Figs. 11 and 12). The EGFP-MBD-NLS fluorescence overlapping well with Hoechst fluorescence was predominantly localized around the rim of the nucleolus in the male pronucleus (Figs. 11A and 12A). In the female

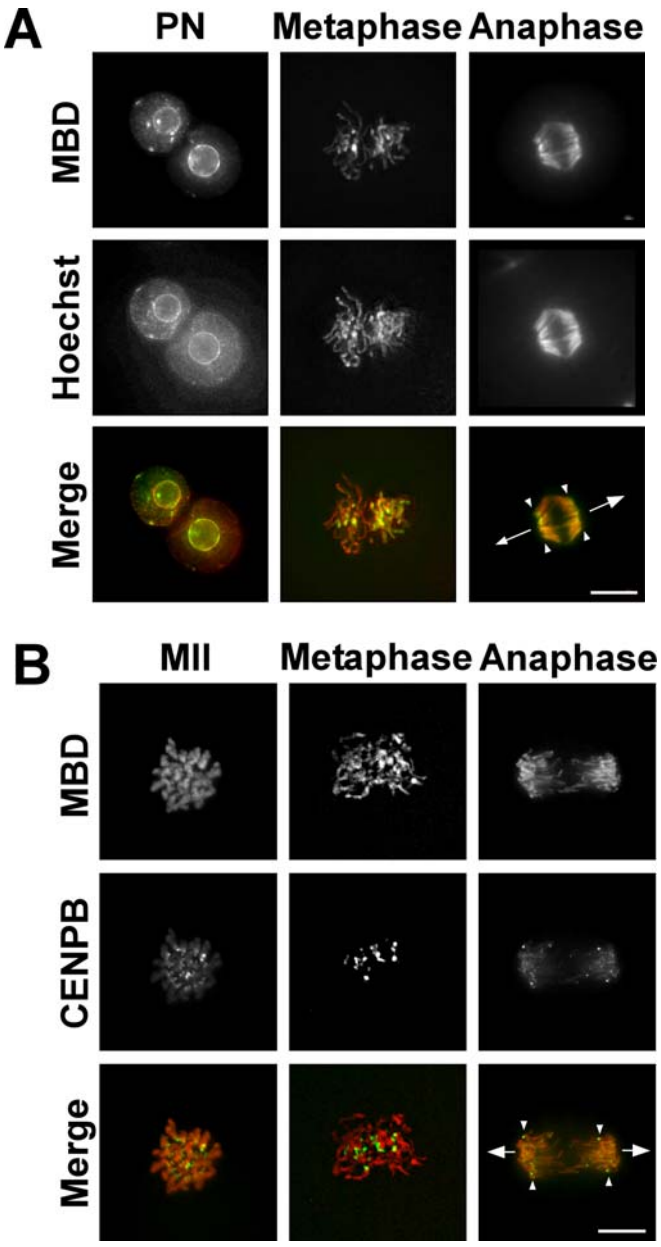

Fig. 11. Localization of methylated DNA in 1-cell to 2-cell transition.
(A) Localization of EGFP-MBD-NLS and Hoechst 33342. Fertilized embryos were recovered 3 h after insemination, and injected with EGFP-MBD-NLS RNA. The 27, 10, and 10 embryos at the pronuclear (PN), metaphase, and anaphase stages, respectively, were stained with Hoechst 33342. The images merged are represented as green and red colors for EGFP-MBD-NLS and Hoechst, respectively. Arrowheads and arrows indicate the localization of the pericentric region (chromocenter) and the direction of chromosomal segregation at the anaphase stage, respectively. Scale bar, 20 μm. (B) Co-visualization of methylated DNA and kinetochore regions. Metaphase II-arrested eggs (MII) or fertilized embryos were co-injected with mRFP-MBD-NLS and CENPB-EGFP RNAs. The 12, 19, and 19 embryos at the MII, metaphase, and anaphase stages, respectively, were examined. The images merged are represented as red and green colors for mRFP-MBD-NLS and CENPB-EGFP, respectively. Scale bar, 20 μm.

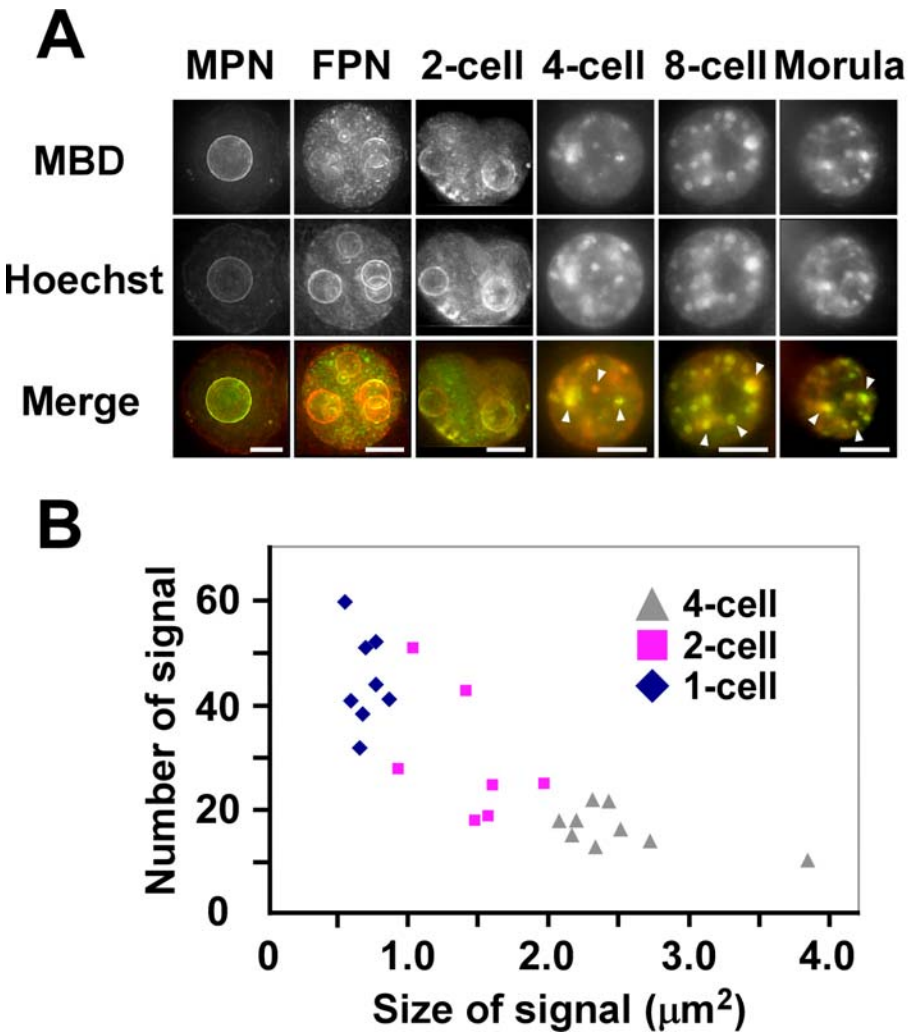

Fig. 12. Dynamic changes of methylated DNA localization in preimplantation embryos.
(A) Presence of EGFP-MBD-NLS fluorescence in the (pro)nuclei of preimplantation embryos. Fertilized embryos were injected with EGFP-MBD-NLS RNA, and then incubated until blastocyst formation. Following counterstaining with Hoechst 33342, 27, 18, 24, 8, and 10 embryos at 1-cell, 2-cell, 4-cell, 8-cell, and morula stages were observed, respectively. The images merged are represented as green and red colors for EGFP-MBD-NLS and Hoechst, respectively. The pericentric heterochromatin foci are indicated by arrowheads. MPN, male pronucleus; FPN, female pronucleus. Scale bar = 10 μm. (B) Change of EGFP-MBD-NLS dotted signals in number and size. The 8, 7, and 9 embryos at the 1-cell, 2-cell, and 4-cell stages were examined, respectively. The average number and size per embryo are plotted.

pronucleus, the nucleoplasm contained small dotted signals of the EGFP fluorescence with sizes of less than 1 μm. The EGFP fluorescence was also detected weakly around the nucleolar rim in the female pronucleus, as found in the male pronucleus. At the metaphase and anaphase stages, the intense EGFP fluorescence was observed in the centromere and kinetochore regions, respectively (Fig. 11A). Labeling of the embryos co-injected with mRFP-MBD-NLS and CENPB-EGFP RNAs verified the highly methylated state of the pericentric region close to the kinetochore region (Fig. 11B).

EGFP-MBD-NLS RNA-injected, fertilized embryos exhibited the fluorescence in the nuclei of 1-cell through morula embryos (Fig. 12A). A sex-specific compartmentalized pattern of the EGFP fluorescence was observed in the (pro)nuclei of 1- and 2-cell embryos, whereas the number and size of the fluorescent signals dramatically changed during the 2-cell to 4-cell transition (Fig. 12B). The fluorescence was detected as dotted and ring-like signals around the nucleoli of embryos at the 1-cell and 2-cell stages, as described in Fig. 11. However, the embryos at the 4-cell, 8-cell, and morula stages only contained the dotted EGFP signals that were bigger than those at the 1-cell and 2-cell stages (Fig. 12A). The EGFP fluorescence overlapped well with Hoechst fluorescence in the embryos at the stages of 1-cell through morula. Intriguingly, the blastocyst-stage embryos contained the EGFP fluorescence not in the nucleus but in the cytoplasm (data not shown). The reason for this phenomenon may be due to the export of EGFP-MBD-NLS from the nucleus to cytoplasm possibly for protein degradation. Thus, the pericentric region may be highly DNA-methylated until the morula-stage embryos. Moreover, the dramatic change of chromatin configuration occurs during the developmental transition from 2-cell to 4-cell embryos, consistent with the previously described data obtained by immunostaining with

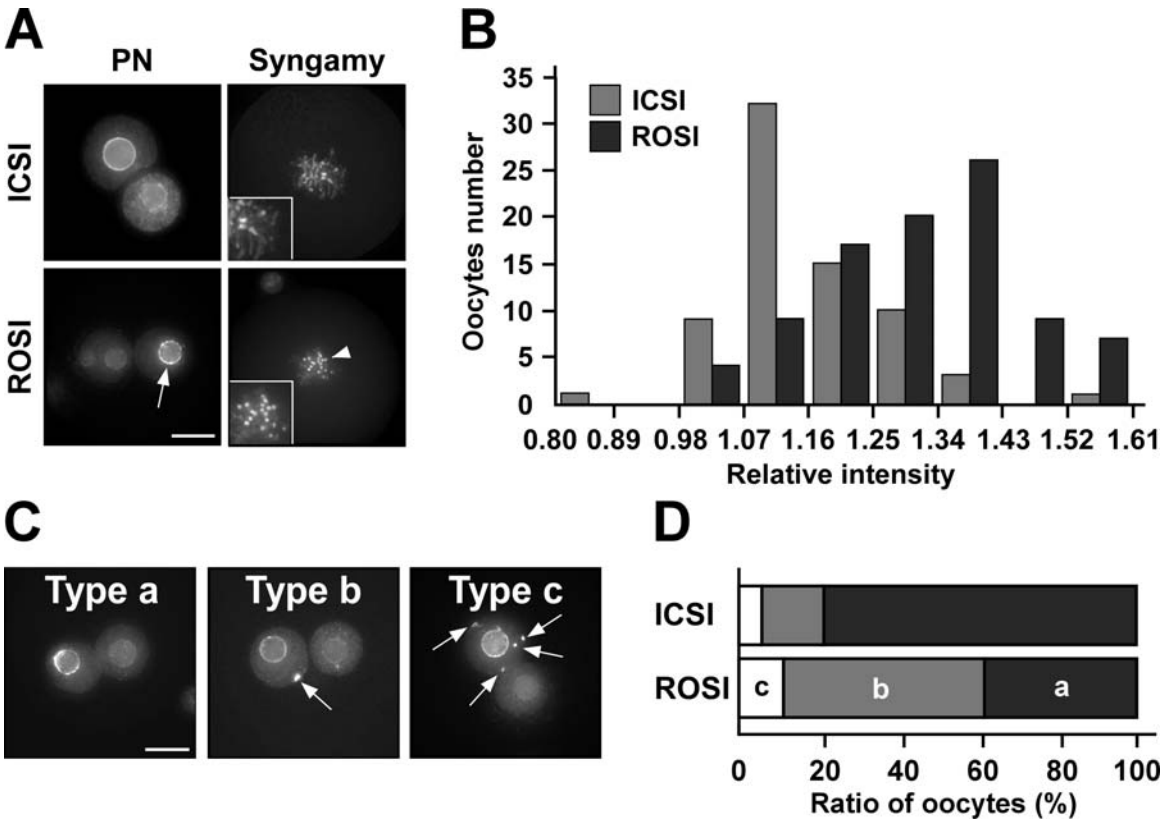

Fig. 13. DNA methylation patterns of ICSI and ROSI embryos.
(A) Fluorescent images of ICSI and ROSI embryos injected with EGFP-MBD-NLS RNA. The embryos at the pronuclear (PN) and syngamy stages (12-15 and 15-20 h after ICSI or ROSI, respectively) were observed. The intense fluorescence of EGFP-MBD-NLS was found in the nucleolar rim of male pronucleus (arrow) and in the pericentric region of the metaphase chromosome (arrowhead) in the ROSI embryos. The magnified images of the male chromosomes are indicated in insets. Note that if one of two pronuclei in a ROSI embryo contained many small dotted signals in the nucleoplasm, and did no intensely fluorescent signals in the nucleolar rim, it was defined as "female pronucleus". Scale bar, 20 μm. (B) Difference of fluorescent intensity in the male nucleoli between ICSI and ROSI embryos. A total of 71 ICSI and 93 ROSI embryos were examined. The fluorescent intensity of the male nucleolus was normalized to that of the female pronucleus in the same embryo. The relative intensity of the male nucleolus in ROSI embryo was significantly higher than that in ICSI embryos (means ± S.E. = 1.32 ± 0.01 and 1.16 ± 0.01, respectively; Student *t*-test, $P<0.0001$). (C) Presence of small, bright dots in the male nucleoplasm of ROSI embryos. Some male pronuclei in ICSI (not shown) and ROSI embryos contained small, bright dots (arrows) scattered only in the nucleoplasm. The ICSI and ROSI embryos were categorized as follows. If the embryo contained no bright dot in the male nucleoplasm, it was defined as "type a". The embryos containing 1-2 and more than 3 dots were classified as "types b and c" embryos, respectively. A weak dotted signal in the male nucleoplasm was treated as a false signal when the intensity of the fluorescent dot in the male nucleoplasm was less than 110% of that in the female nucleoplasm. Scale bar, 20 μm. (D) Increased ratio of scattered bright dot-containing embryos in ROSI embryos. The numbers of type a, type b, and type c embryos were counted 12-15 h after ICSI or ROSI.

Table 2.

Correlation between the presence of scattered fluorescent dots in the male nucleus and embryonic development of ROSI embryos.

No. (%) of embryo				No. (%) of embryo developed to					
Survived by ROSI	Surived by RNA injection	Formation of two pronuclei	Cell type	PN	2-cell	4-cell	8-cell	Morula	Blastocyst
267/334 (79.9)	206/265 (77.7)	110/202 (54.4)	a	35 (100)	25 (71.4)	25 (71.4)	25 (71.4)	23 (65.7)	17 (48.6)
			b	47 (100)	25 (53.2)	24 (51.1)	23 (48.9)	22 (46.8)	12 (25.5)
			c	11 (100)	4 (36.4)	4 (36.4)	4 (36.4)	3 (27.3)	2 (18.2)

EGFP-MBD-NLS RNA (1 ng/μl) was injected into ROSI embryos.

Cell type assessment was carried out at the pronuclear (PN) stage, and the ROSI embryos were then developed into blastocysts by culture *in vitro* for 72 h.

anti-HP1β and anti-centromere antibodies (Martin et al., 2006).

Importance of methylated DNA assembly in male pronucleus for development

To examine the difference of DNA methylation states in the nuclei between ICSI and ROSI embryos, EGFP-MBD-NLS fluorescence was observed at the pronuclear and syngamy stages (Fig. 13A). Although the patterns were similar to each other, the EGFP fluorescence in the male nucleolus of ROSI embryos was more intense than that of ICSI embryos (Fig. 13B). Some ICSI and ROSI embryos contained small, bright dots scattered only in the male nucleoplasm (Fig. 13C). When the embryos were classified into three groups (types a, b, and c) on the basis of the numbers of the scattered dots, the ROSI embryo was distinguished from the ICSI embryo by an increased proportion of type-b and type-c embryos containing 1-2 and more than 3 dots in the male nucleoplasm, respectively (Fig. 13D).

Following measurements of the fluorescent intensity and number of scattered fluorescent dots at the pronuclear stage, ROSI embryos were developed into blastocysts by culture for 72 h (Table 2). Of 93 ROSI embryos examined, 31 embryos developed into blastocysts. No significant correlation was found between the number of embryos developed into blastocysts and the fluorescent intensity in the male nucleolus (data not shown). Cell-type assessment indicated that 35, 47, and 11 ROSI embryos correspond to the type-a, type-b, and type-c embryos at the pronuclear stage, respectively (Table 2). The type-a embryos showed a significantly high rate of 2-cell formation (71%, 25/35 embryos), whereas only 53% (25/47 embryos) and 36% (4/11 embryos) of the type-b and type-c embryos developed into 2-cell embryos, respectively. These results may suggest the

importance of the methylated DNA assembly in the nucleolus of male pronucleus for the embryonic development.

DISCUSSION

In this study, I employed a synthetic RNA encoding EGFP or mRFP fused to MBD and NLS of human MBD1. The reason for the use of only MBD and NLS instead of the entire region of MBD1 is because one of the Cys-rich CXXC domains of MBD1 is known to interact with chromatin assembly factor-1 (CAF-1) that facilitates the nucleosome assembly of newly replicated DNA *in vitro* (Sarraf S.A. et al., 2004). Two other proteins, histone H3 methyltransferase Suv39h1 and methyl lysine-binding protein HP1, have also been reported to interact directly with MBD of MBD1 in cells (Fujita et al., 2003). The localization of MBD1 (MBD-NLS) in the nucleus is not altered by Suv39h1 and HP1α, although MBD is capable of tethering the Suv39h1-HP1α complex to the methylated DNA region (Fujita et al., 2003). Indeed, our preliminary data indicate that the fluorescent signal of mRFP-HP1β is abundantly present in both nucleoplasm and nucleolus of the male and female pronuclei in the fertilized embryos, as is in the case of immunostaining using anti-HP1β antibody (Santos et al., 2005), and that the mRFP-HP1β localization is shifted to the nucleolar rim by co-expression with EGFP-MBD-NLS (data not shown). Thus, it is most likely that EGFP-MBD-NLS is localized in the methylated DNA region of chromatin in cells.

The fluorescence of EGFP-MBD-NLS is intensely observed both in the central region of decondensing sperm nucleus (Fig. 9), and in the rim region of the nucleolus in the male pronucleus (Figs. 11 and 12). FISH analysis has previously demonstrated that the major satellite DNA sequence is localized in the same regions of decondensing sperm and pronucleus (Arney et al., 2002; Dozortsev et al., 2000; Haaf and Ward, 1995; Pittoggi et al., 1999).

Moreover, these two regions have been shown to react with autoimmune sera from CREST scleroderma patients that recognize inner kinetochore proteins (Cowell et al., 2002; Schatten et al., 1988). Indeed, the intense fluorescence of mRFP-MBD-NLS is found near the centromere and kinetochore regions recognized by CENPB-EGFP at the metaphase and anaphase stages of fertilized embryos, respectively (Fig. 11). These results suggest that the pericentric region recognized by EGFP-MBD-NLS may be highly methylated at the pronuclear stage, as compared with other genomic regions. Although the pericentric heterochromatin in NIH3T3 cultured cells is methylated (Fig. 8), comparative analysis of the fluorescent intensity between the centromeric and other chromosomal regions reveals that the level of DNA methylation in cultured cells is much higher than that in the fertilized embryos (Figs. 8 and 11). In the female pronucleus, a large number of small dotted signals of the EGFP-MBD-NLS fluorescence are present in the nucleoplasm, while the rim region of the nucleolus exhibits a weak fluorescence (Figs. 11 and 12). Since the small fluorescent dots do not overlap with Hoechst fluorescence, euchromatin and/or facultative heterochromatin may be highly DNA-methylated only in the female pronucleus.

A differential reprogramming of parental genomes is thought to proceed within the same oocyte cytoplasm during pronuclear formation. DNA demethylation of the paternal genome occurs soon after fertilization, whereas the maternal genome is resistant to demethylation and/or exhibits de novo methylation (Mayer et al., 2000; Santos et al., 2002 and 2005). The male pronucleus is completely demethylated 4-8 h after fertilization when the DNA methylation state is assessed by using anti-5mC antibody (Mayer et al., 2000; Santos et al., 2002 and 2005). In this study, consistent with the previous observation (Mayer et al., 2000; Santos et al., 2002 and 2005), the paternal

genome undergoes active DNA demethylation in the enlarging male pronucleus (Fig. 10). However, the methylated paternal genome is dispersed, assembled, and then migrated to the nucleolar rim within the male pronucleus 4-8 h after insemination (Fig. 9). Thus, the dynamic movement of the methylated chromatin occurs together with DNA demethylation during male pronuclear enlargement. The paternal genome may be distinguished from the maternal genome by the localization of methylated DNA during pronuclear formation; the male and female pronuclei contain methylated DNA predominantly in the nucleolar rim and nucleoplasm, respectively.

Our data indicate that a configurational change of methylated chromatin dramatically occurs during the transition of 2-cell to 4-cell embryos (Fig. 12). The DNA methylation state in the 2-cell embryo resembles that in the female pronucleus at the 1-cell stage, whereas the 4-cell, 8-cell, and morula embryos contain many large dots likely corresponding to the pericentric heterochromatin in the nuclei. Because the DNA methylation pattern in the 4-cell embryo is essentially similar to that in somatic cells (Coffigny et al., 1999; Marchal et al., 2004; Martin et al., 2006), the 2-cell embryo may still possess the chromatin configuration characteristic of the pronuclear-stage embryo. In some experiments, I have examined the DNA methylation pattern of 4-cell embryos previously treated with transcriptional inhibitor α-amanitin (25 μg/ml) using the EGFP-MBD-NLS RNA-injection method (data not shown). The sizes of EGFP fluorescent signals in the amanitin-treated 4-cell embryos were approximately twice as small as those in the untreated embryos. No significant difference was found in the signal number between the 4-cell embryos with and without the amanitin treatment. These results imply that the dynamic change of the chromatin configuration in the 2-cell to 4-cell transition is retarded by transcriptional suppression. Thus,

the early transcripts (Hamatani et al., 2004) and/or transcription machinery may be involved in the remodeling of chromatin.

More recently, an epigenetic abnormality has been reported to occur in the paternal genome of ROSI embryo during pronuclear formation (Kishigami et al., 2006). When methylated DNA was probed by anti-5mC antibody, the paternal genome in the ROSI embryo was apparently demethylated and remethylated 6 and 10 h after round spermatid injection, respectively, assuming that a low rate of embryonic development of the ROSI embryos (Ogura et al., 2001) is possibly due to the DNA remethylation (Kishigami et al., 2006). In this study, I have verified a higher level of DNA methylation in the paternal genome of ROSI embryo than of ICSI embryo 12-15 h after injection (Fig. 13). However, our data imply that the poor embryonic development of the ROSI embryos, particularly the 1-cell to 2-cell development (Table 2), may result from the abnormal localization of methylated chromatin in the nucleoplasm of male pronucleus rather than from the high level of DNA methylation in the paternal genome (Fig. 13). Since the nuclear architecture and chromosomal territories are known to affect gene expression (Cremer and Cremer, 2001; Gasser, 2002), the proper arrangement of methylated DNA is presumably essential for zygotic gene expression during pronuclear formation. The mislocalized dotted structure in the nucleoplasm of male pronucleus (Fig. 13) may correspond to the pericentric region that failed to be recruited to the nucleolus during pronuclear formation. Because the ROSI embryos contain more abnormal bright dots than the ICSI embryos (Fig. 13), formation of the dotted structure may result from the difference of chromatin components, histone and protamine, between the ROSI and ICSI embryos.

Here I show the usefulness of live-cell imaging technique for

understanding the molecular mechanism of genome reprogramming in mouse preimplantation embryos. This technique may be applicable to the research fields of medical care and animal industries, because the embryos are still alive and are capable of developing to offspring even after fluorescent microscopic observation, in addition to no transgenesis due to the RNA injection (Yamagata et al., 2005).

CHAPTER III

Centromeric DNA Hypomethylation As an Epigenetic Signature Discriminates Between Germ and Somatic Cell Lineages

SUMMARY

Germ cells have unique features strikingly distinguishable from somatic cells. The functional divergence between these two cell lineages has been postulated to result from epigenetic mechanisms. Here I show that the chromosomal centric and pericentric (C/P) regions in male and female germline cells are specifically DNA-hypomethylated, despite the hypermethylation status in somatic cells. In multipotent germline stem cells, the C/P region was initially hypomethylated and then shifted to the hypermethylation status during differentiation into somatic lineage *in vitro*. Moreover, the somatic-type hypermethylation pattern was maintained in the somatic cell-derived nuclear transfer embryos throughout preimplantation development. These results imply that the identity of germ cell lineage may be warranted by the hypomethylation status of the C/P region as an epigenetic signature.

INTRODUCTION

Germ cells capable of transmitting genetic information to next generation have the totipotency acquired by germ cell-specific nuclear events, including meiotic division and global reprogramming processes. In mouse embryogenesis, primordial germ cells (PGCs), which are present in a posterior region of the primitive streak in the extra-embryonic mesoderm, migrate into the embryonic mesoderm, enter into the genital ridge at embryonic day 10.5 (E10.5), and continue to proliferate mitotically until E13.5. Female PGCs enter the prophase of first meiotic division around E13.5, where they are arrested until the later stages during the postnatal life (McLaren, 1994). Male PGCs, on the other hand, enter the mitotic arrest around E13.5 and resume proliferation postnatally. Germ cells are distinguished from somatic cells by histological characteristics and specific gene expression during embryogenesis (Extavour and Akam, 2003). It is also known that the epigenetic features of germ and somatic cells discriminate between these two cell lineages (Shiota et al., 2002). However, the definitive conclusion on the epigenetic regulation has not yet been drawn.

Cytosine methylation of CpG dinucleotides is a major epigenetic modification of DNA, and plays a crucial role(s) in gene regulation such as X chromosome inactivation, genome imprinting, and inactivation of transposable elements (Li, 2002). *De novo* methylation of particular genes is also thought to control the cell differentiation process during embryogenesis (Reik et al., 2001). In this study, to elucidate the epigenetic features involved in the functional divergences between germ and somatic cells, I have focused on the DNA methylation status of chromosomal centric and pericentric (C/P) regions, owing to germ cell-dominant expression of the

pericentric transcripts (She et al., 2004).

MATERIALS AND METHODS

Southern blot analysis

Frozen mouse tissues (0.1 g) were crushed, placed in a lysis buffer (1 ml) consisting of 50 mM Tris/HCl, pH 8.0, 0.1 M NaCl, 20 mM EDTA, 1% SDS, proteinase K (0.1 mg/ml), and RNase A (0.08 mg/ml), and incubated at 50°C with gentle rocking overnight. In epididymal sperm, 2-mercaptoethanol was added to the lysis buffer at a final concentration of 0.5% to reduce the disulfide bonds of the nucleoproteins. Genomic DNA was extracted with phenol-chloroform, precipitated with ethanol, and dissolved in 10 mM Tris/HCl, pH 8.0, containing 1 mM EDTA (TE). The DNA samples were digested at 37°C with Msp I or Hpa II, separated by electrophoresis on agarose gels (50 ng DNA/lane), transferred to Hybond-N^+ membranes (GE Healthcare Bio-Sciences, Piscataway, NJ), and hybridized to ^{32}P-labeled probes at 55°C overnight, as described previously (Kashiwabara et al., 2002). The DNA probes were amplified by polymerase chain reaction (PCR) using the following sets of oligonucleotide primers: 5’-GACGACTTGAAAAATGACGAAATC-3’ and 5’-CATATTCCAGGTCCTTCAGTGTGC-3’ for major satellite; 5’-CATGGAAAATGATAAAAACC-3’ and 5’-CATCTAATATGTTCTACAGTGTGG-3’ for minor satellite; 5’-ACATTCGCCGTTACAAGATGGCGCTGA-3’ and 5’-AATTGTTATTAGACGCGTTCTCACGCC-3’ for intracisternal A particle (IAP); 5’-ATCTTGGTCCCGGGACTCCAAGGAACTTA-3’ and 5’-GTTAGTAGTTATAGTTGACTCTGTTTAGAG-3’ for long interspersed nuclear elements 1 (LINE1 or L1 sequences).

Cell collection

Preimplantation embryos were prepared by fertilizing epididymal sperm with metaphase II-arrested eggs from 8-week-old ICR mice (Japan SLC, Shizuoka, Japan) *in vitro*, and incubated in KSOM medium (Lawitts and Biggers, 1993), as described previously (Yamagata et al., 2005). Embryos at E6.5, E7.5, and E10.5 were obtained from the uterus of naturally mated ICR mice. Spermatogenic cells were dispersed from seminiferous tubules of ICR mice in Hepes/CZB medium (Kimura and Yanagimachi, 1995) by gentle pipetting, separated into various differentiation stages, and collected one by one according to the cell morphology and nuclear size, using a micromanipulator (Ogura and Yanagimachi, 1993). Cloned embryos were prepared using B6D2F1 female mice as donors and recipients, as described previously (Wakayama et al., 1998). The embryos produced by *in vitro* fertilization (IVF) of metaphase II-arrested eggs and epididymal sperm from C57BL/6Cr and DBA/2 mice, respectively, were used as controls. PGCs were collected from E10.5 and E13.5 embryos obtained by natural mating between B6D2F1 female and Oct-4/EGFP transgenic male mice (GOF-18/delta PE/GFP, 129/Sv-ter background), as described previously (Miki et al., 2005). Multipotent germline stem (mGS) cells were treated with trypsin, placed in ES medium (Dulbecco's modified Eagle's medium, Invitrogen) free from leukemia inhibitory factor in bacterial Petri dishes, and cultured for 6 days. Embryoid bodies (EB) with size of more than 200 μm, corresponding to the outer layers of the endoderm surrounding solid cores of ectodermal cells, were harvested from the cell aggregates. Germline stem (GS) and mGS cells were kind gifts from Dr. T. Shinohara (Kyoto University). All animal experiments were carried out according to the Guide for the Care and Use of Laboratory Animals in University of Tsukuba.

Bisulfite sequencing

Cells were suspended in 20 μl of above lysis buffer (TE for genomic DNA) containing 1 μg salmon sperm DNA as a carrier, incubated at 50°C for 180 min, and subjected to bisulfite modification using an EZ DNA Methylation-Gold kit (Zymo Research, Orange, CA). After dilution with TE (20 μl), an aliquot (2 μl) of the DNA solution was PCR-amplified using the following sets of primers: 5'-GGAATATGGTAAGAAAATTGAAAATTATGG-3' and 5'-CCATATTCCAAATCCTTCAATATACATTTC-3' for major satellite; 5'-TAGAATATATTAGATGAGTGAGTTATATTG-3' and 5'-ATTATAACTCATTAATATACACTATTCTAC-3' for minor satellite; 5'-TTGATAGTTGTGTTTTAAGTGGTAAATAAA-3' and 5'-AAAACACCACAAACCAAAATCTTCTAC-3' for IAP. The PCR reaction was carried out by 35 cycles of 95°C for 30 s, 58°C for 60 s, and 68°C for 20 s. The amplified DNA fragments were subcloned into a pGEM-T Easy vector (Promega, Madison, WI), and at least 4 subclones (usually 6-8 subclones) derived from each of the bisulfite-treated genomic DNAs were sequenced using an ABI 3100-Avant Genetic Analyzer (Applied Biosystems, Foster City, CA). Two independent genomic DNA preparations from each group of cells (three DNA samples for spermatogenic cells, ES cells, GS cells, and mGS cells) were bisulfite-treated and PCR-amplified once, using metaphase II-arrested egg and liver DNAs containing the hypomethylated and hypermethylated C/P regions, respectively, as controls. For morulae and blastocysts reconstructed by transfer of somatic cell nucleus (SCN), a genomic DNA sample was bisulfite-treated, PCR-amplified twice, and then subjected to sequencing analysis, because of the difficulty in

obtaining these cells of sufficient quantity.

Live-cell imaging

Synthetic RNAs encoding enhanced green fluorescence protein (EGFP) or monomeric red fluorescence protein (mDsRed) fused to a part of human methyl CpG binding protein 1 (Fujita et al., 1999) containing the methyl CpG binding domain (MBD) and nuclear localization signal (NLS), and fused to the DNA-binding domain of human CENP-B (Shelby et al., 1996) were prepared as described previously (Yamagata et al., 2005; Yamazaki et al., 2007). RNA microinjection into metaphase II-arrested eggs and time-lapse observation of cells were carried out as described previously (Yamagata et al., 2005; Yamazaki et al., 2007). Following RNA injection, cumulus cell nuclei were microinjected into the metaphase II-arrested eggs without metaphase-plate enucleation by a piezo-assisted micromanipulator (PrimeTech, Ibaraki, Japan). The reconstructed embryos were activated by 5 mM $SrCl_2$ in the presence of 5 μg/ml cytochalasin B to prevent the polar body extrusion, and observed under a conventional fluorescence microscope (Olympus IX-71, Tokyo, Japan) or a Nipkow-disk scanning confocal microscope (CSU10, Yokogawa Electric, Tokyo, Japan).

RESULTS AND DISCUSSION

DNA methylation status of major and minor satellites in mouse tissues, sperm, and egg

Two types of repeat sequences, major and minor satellites, are present in the pericentric and centric regions of mouse chromosomes, respectively (Guenatri et al., 2004) (Fig. 14A). Consistent with a previous report (Sanford et al., 1984), Southern blot analysis using CpG methylation-sensitive HpaII and insensitive MspI indicated that these two satellites are hypermethylated in all adult mouse tissues and cells tested, except the testis and epididymal sperm (Fig. 14B). However, endogenous retroviral repetitive elements uniformly spreading over the entire chromosome, such as IAP and LINE1, were highly methylated in all tissues including the testis and sperm (Fig. 14B). Bisulfite sequencing analysis also revealed that the two satellites in both sperm and metaphase II-arrested eggs are hypomethylated, but those in cumulus cells are hypermethylated (Fig. 15). Thus, male and female gametes are unique in possessing the hypomethylated C/P region.

CpG methylation levels of major and minor satellites in various germline cells

When the levels of CpG methylation in pre- and post-implantation embryos were examined, the hypomethylated status persisted throughout preimplantation development (Fig. 16A). Both *de novo* methylation of the major and minor satellites and remethylation of IAP started after the blastocyst stage. These data suggest that *de novo* methylation of the C/P region associated with the genome-wide remethylation may be implicated in the establishment of the somatic cell lineage.

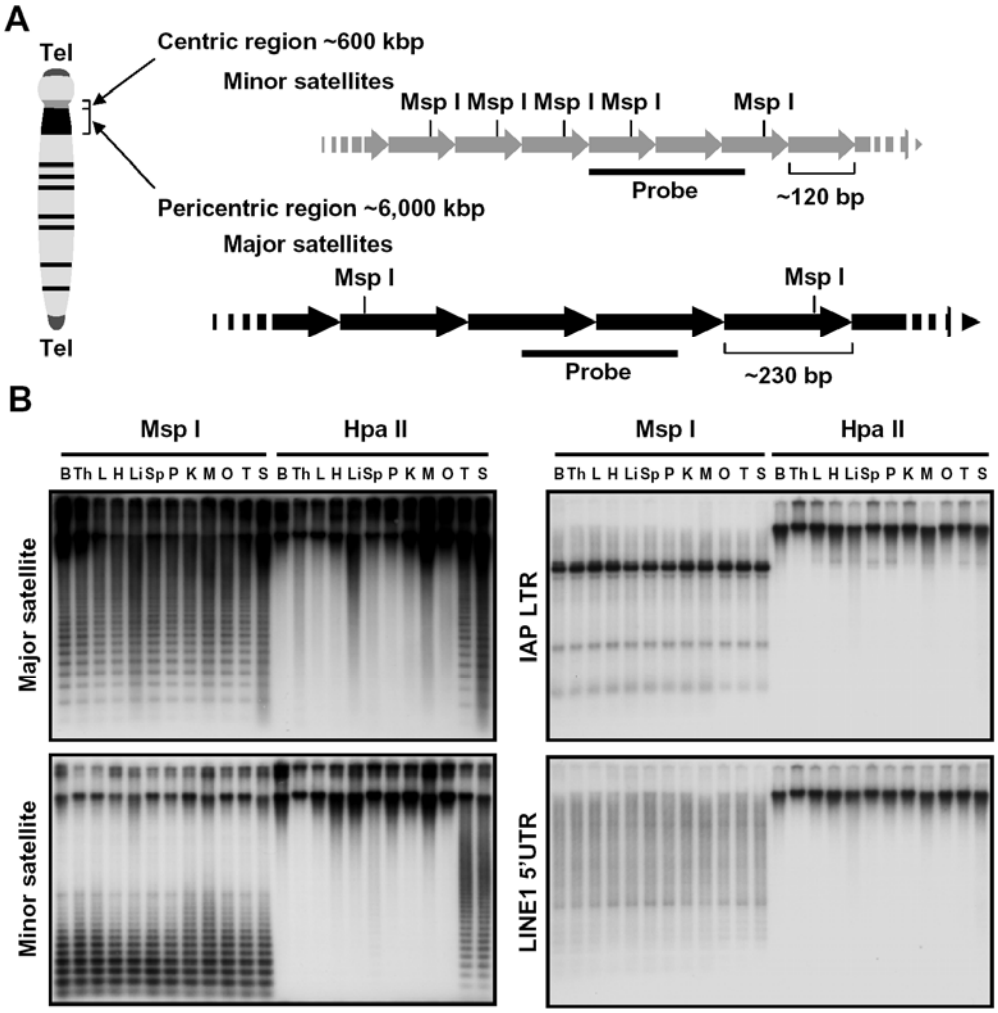

Fig. 14. DNA methylation status of major and minor satellites in mouse tissues.
(A) The C/P region containing the major and minor satellites on mouse chromosome. The minor satellites consisting of 120-bp monomers (arrows) are tandemly repeated over approximately 600 kbp on the chromosome. The major satellite region (approximately 6,000 kbp) is formed by 230-bp monomer repeats. Bars represent the DNA probes for Southern blot analysis. Note that the MspI site (CCGG) is frequently present in the minor satellite. Tel, telomere. (B) Southern blot analysis. Mouse genomic DNAs from various tissues and epididymal sperm were digested with methylation-sensitive (HpaII) or insensitive (MspI) restriction enzyme, and hybridized to DNA fragments of the major satellite, minor satellite, IAP LTR, and 5'-untranslated region of LINE1 (5'UTR). B, brain; Th, thymus; L, lung; H, heart; Li, liver; Sp, spleen; P, pancreas; K, kidney; M, muscle; O, ovary; T, testis: S, sperm.

To examine the time when the hypomethylation status is established in the germ cell lineage, genomic DNAs from spermatogenic cells and PGCs were analyzed by bisulfite sequencing. The major and minor satellites of pachytene spermatocytes, and round and elongating spermatids were hypomethylated (Fig. 16B). The methylation levels of the major and minor satellites and IAP in spermatogenic cells and epididymal sperm (approximately 30-40, 40-50, and 90%, respectively) were consistent well with those in newborn prospermatogonia (Kato et al., 2007), suggesting that DNA methylation of the major and minor satellites may be maintained throughout spermatogenesis. Moreover, the difference in the methylation levels of the major and minor satellites among epididymal sperm (approximately 40-50%), metaphase II-arrested eggs (20%), and pronuclear-stage embryos (20%) (Figs. 15B, 16A, and 16B) may be explained by the fact that the methylated paternal genome in the enlarging pronucleus undergoes DNA demethylation 6-12 h after insemination (Mayer et al., 2000; Santos et al., 2002). Indeed, I analyzed the pronuclear-stage embryos prepared at 12-15 h after insemination.

PGCs at E10.5 and E13.5 contained the hypermethylated and hypomethylated satellites, respectively (Fig. 16C). As compared with the major and minor satellites, IAP of the PGC genome was moderately demethylated between the E10.5 and E13.5 stages (Fig. 16C) consistent with the previously reported data (Hajkova et al., 2002). Global DNA demethylation is known to occur in the PGC genome between E8.0 and E12.5 (Seki et al., 2005). Our results therefore suggest that the C/P region of germline cells may be predominantly demethylated in the global demethylation process, likely soon after E10.5, and that the hypomethylation status of the C/P region may be retained throughout gametogenesis and

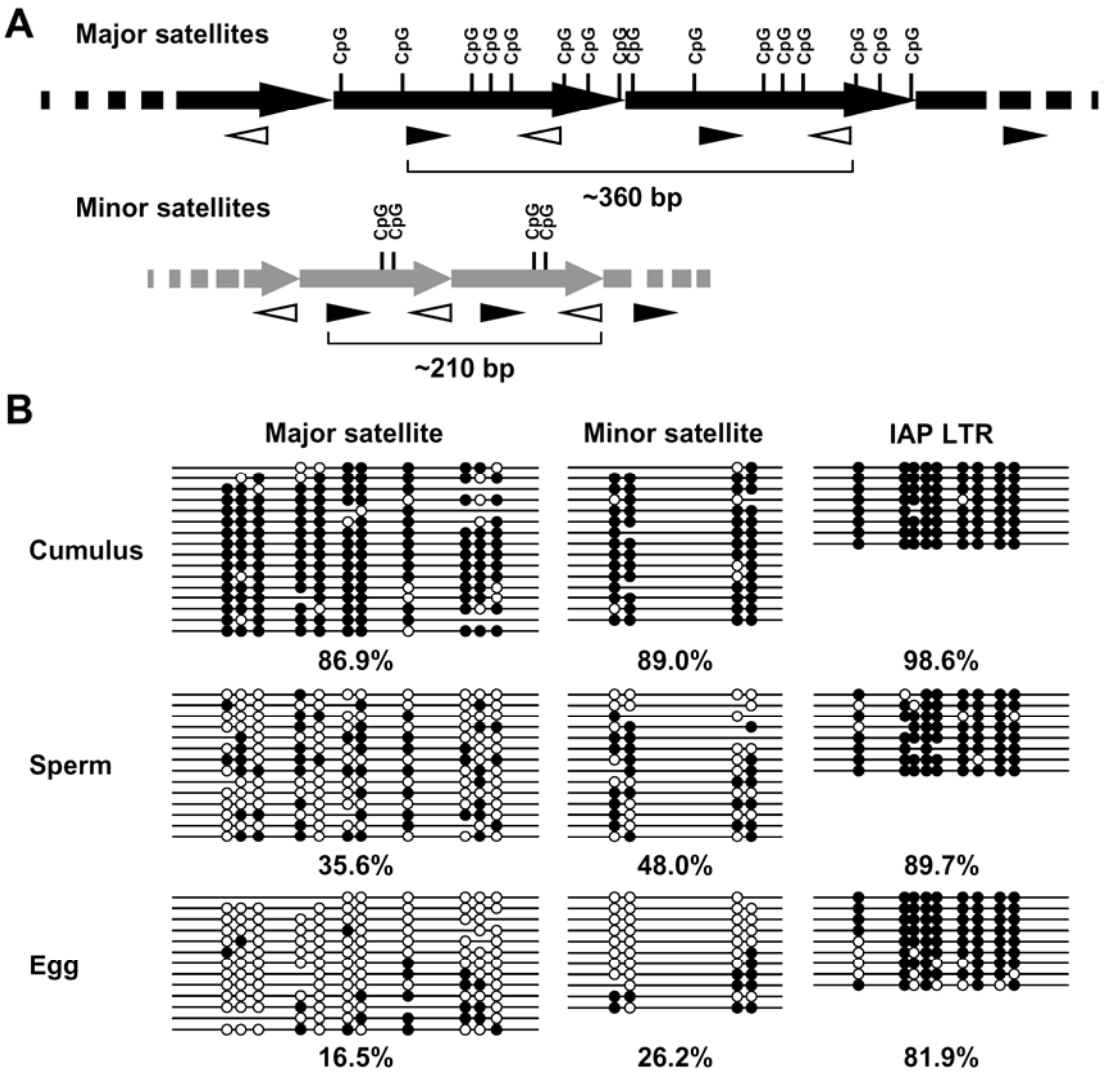

Fig. 15. Bisulfite sequencing of CpG sites in the major and minor satellites of sperm and egg genomes.

(A) CpG loci of the major and minor satellites. Closed and open arrowheads represent the oligonucleotide primers used for bisulfite sequencing. The 360- and 210-bp PCR-amplified fragments containing the 11 and 4 CpG sites in the major and minor satellites, respectively, were subcloned and sequenced. (B) Bisulfite sequencing of CpG sites in the major and minor satellites of sperm and egg genomes. Methylation patterns of the major and minor satellites and IAP LTR in mouse cumulus cells, cauda epididymal sperm, and metaphase II-arrested eggs were examined. Closed and open circles indicate the methylated and unmethylated CpG sites, respectively. Data are represented as % of methylated CpG sites per total CpG sites.

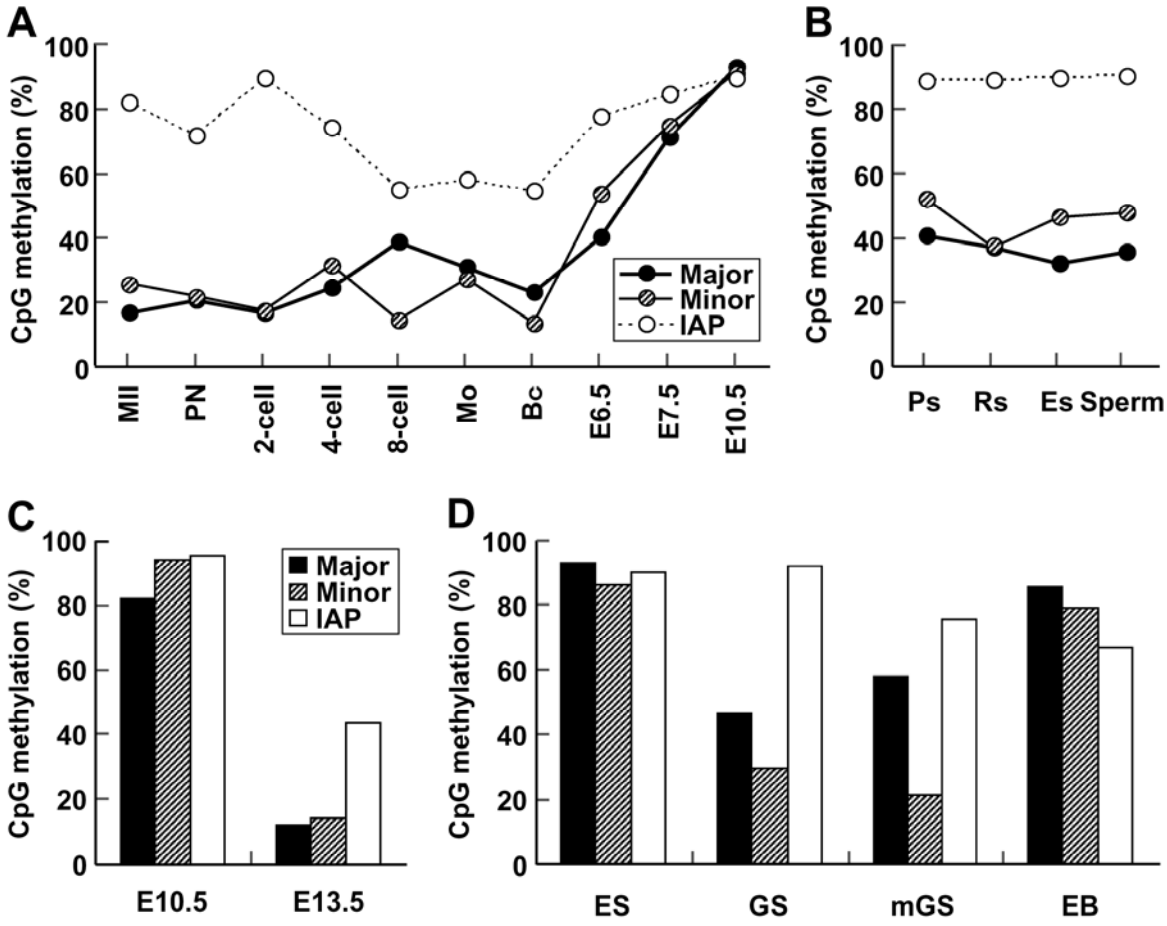

Fig. 16. CpG Methylation levels of major and minor satellites in various germline cells.

The CpG methylation status of the major satellite (closed circles and boxes), minor satellite (hatched circles and boxes), and IAP (open circles and boxes) was analyzed by bisulfite sequencing. The methylation levels of the pre- and post-implantation embryos (A), spermatogenic cells (B), developing PGC (C), and stem cell lines (D) are shown as % of methylated CpG sites per total CpG sites. MII, metaphase II-arrested egg; PN, pronuclear-stage embryo; Mo, morula; Bc, blastocyst; E6.5, embryo at day 6.5; Ps, pachytene spermatocyte; Rs, round spermatid; Es, elongating spermatid; ES, embryonic stem cell; GS, germline stem cell; mGS, multipotent germline stem cell; EB, embryoid body differentiated from mGS cells *in vitro*.

preimplantation development. Because germline cells have been demonstrated to appear in proximal epiblast at E6.25 (Ohinata et al., 2005), it is conceivable that germline cells are further specified by the hypomethylation status of the C/P region at least 4 days after their first appearance.

The DNA methylation level of the C/P region was relatively low in GS and mGS cells from neonatal mouse testis (Kanatsu-Shinohara et al., 2003 and 2004), despite the hypermethylation status of pluripotent embryonic stem (ES) cells (Fig. 16D). However, the C/P region of EB differentiated from mGS cells *in vitro* was hypermethylated. These data emphasize that the germ cell lineage may maintain the hypomethylation status of the C/P region as an "epigenetic signature."

Methylation status of the C/P region in embryos reconstructed by somatic cell nuclear transfer and fertilization in vitro

Although the technology of somatic cell cloning is established, several issues still remain to be addressed: an extremely low level of the cloning efficiency (Wakayama et al., 1998) and aberrant phenotypes (Wakayama and Yanagimachi, 1999; Ogonuki et al., 2002; Tamashiro et al., 2002). These abnormalities probably result from incomplete reprogramming of SCN, because unusual DNA methylation patterns have been found in the preimplantation embryos of domestic animals by immunostaining (Dean et al., 2001; Beaujean et al., 2004) and bisulfite sequencing (Kang et al., 2001). I thus examined the methylation status of the C/P region in SCN at 1-cell embryo stage by live-cell imaging (Figs. 17 and 18). DNA methylation was visualized by injection of synthetic RNA encoding EGFP-MBD-NLS or mDsRed-MBD-NLS into metaphase II-arrested eggs (Yamagata et al., 2005; Yamazaki et al., 2007).

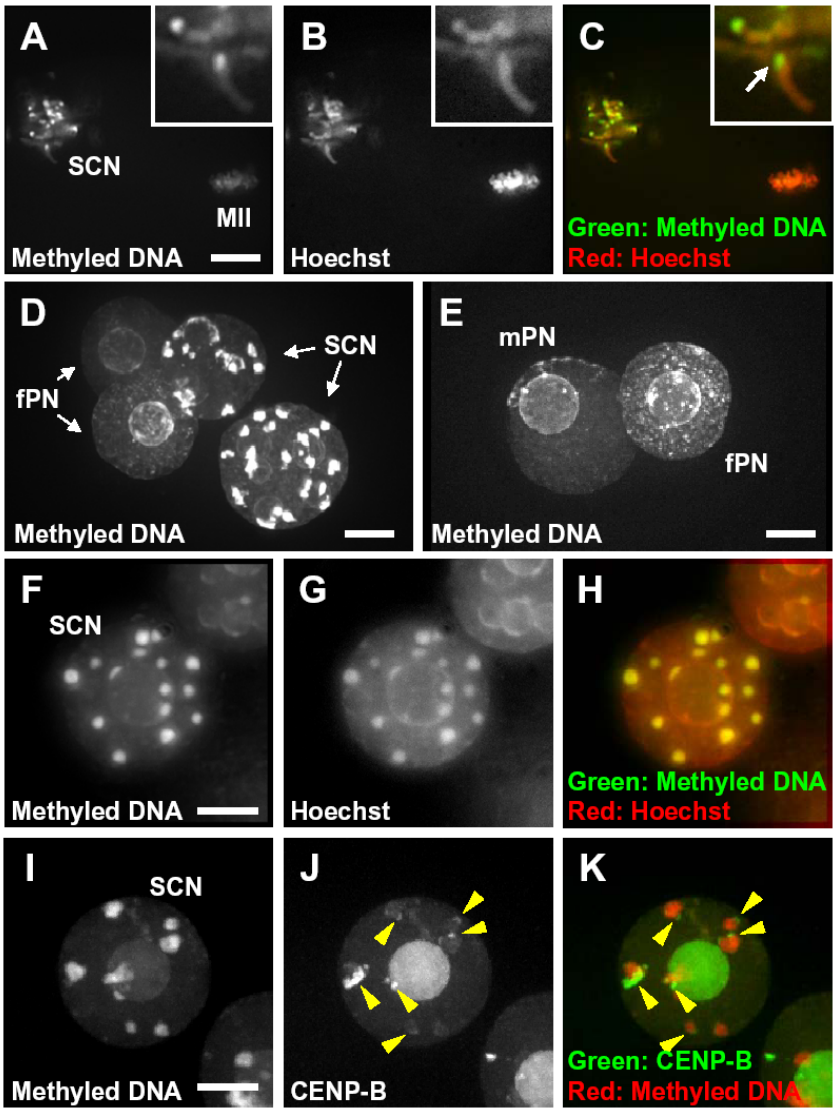

Fig. 17. DNA methylation status of the C/P region in embryos reconstructed by SCNT and IVF.

Metaphase II-arrested eggs were injected with synthetic RNA encoding EGFP (mDsRed)-MBD-NLS or CENPB-EGFP and then with the nuclei of cumulus cells (SCN), and analyzed by live-cell imaging. (A, B, and C) Live-cell imaging of EGFP-MBD-NLS at the metaphase stage. The methylated DNA region was visualized by the EGFP-MBD-NLS fluorescent signals. The embryos were co-stained with Hoechst 33342. Insets indicate the magnified images of the SCN chromosomes, and an arrow represents the highly methylated region in the distal end of the SCN chromosome. MII, metaphase II-plate. (D and E) Live-cell imaging of EGFP-MBD-NLS at the interphase stage. The 1-cell embryos reconstructed by SCNT (D) and IVF (E) were analyzed. fPN, female pronucleus; mPN, male pronucleus. (F-K) Highly methylated region in SCN at the interphase stage. The methylated DNA and centromeres in SCN were co-visualized by EGFP- or mDsRed-MBD-NLS and CENPB-EGFP (arrowheads), respectively. Scale bar , 10 μm.

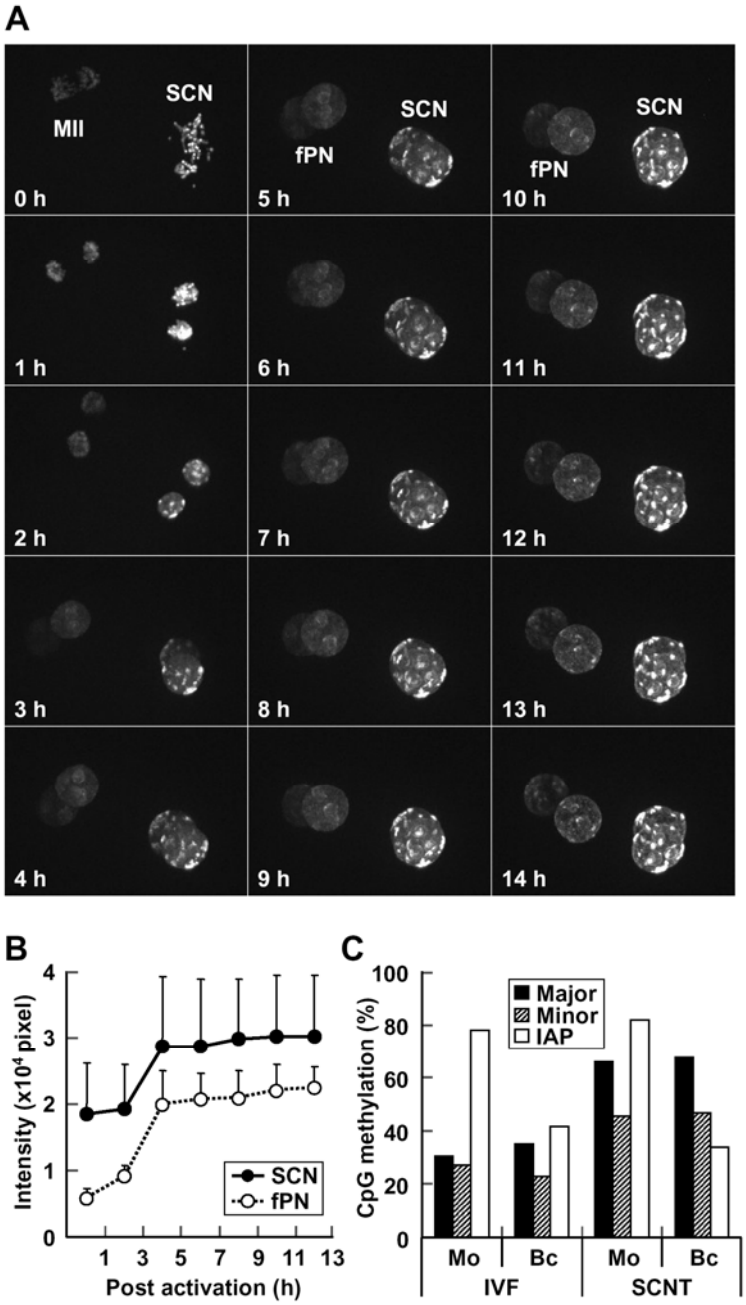

Fig. 18. DNA methylation status of the C/P region in SCNT and IVF embryos during preimplantation development.
(A) Time-lapse imaging of EGFP-MBD-NLS in the SCN-derived pseudopronucleus and female pronucleus (fPN) of 1-cell embryo. The EGFP-MBD-NLS signals were monitored after egg activation. MII, metaphase plate. (B) SCN maintains a high level of EGFP-MBD-NLS fluorescence during pronuclear formation. Total fluorescent intensities of the (pseudo)pronuclei after egg activation were measured. (C) Bisulfite sequencing of the repetitive elements of morula- (Mo) and blastocyst-stage (Bc) embryos reconstructed by IVF or SCNT of cumulus nuclei. Data are represented as % of methylated CpG sites per total CpG sites.

As compared with metaphase-II plate, the distal ends of chromosomal arms corresponding to the centromere region of metaphase-synchronized SCN showed a significantly high level of the EGFP-MBD-NLS fluorescence (Figs. 17A, B, and C). Following artificial egg activation, a large number of intensely fluorescent foci were observed in the SCN-derived pseudopronuclei of the 1-cell embryos reconstructed by SCN transfer (SCNT, see Fig. 17D). In contrast, the fluorescent levels of small dots in the male and female pronuclei of 1-cell embryos produced by IVF were very low (Fig. 17E). The EGFP-MBD-NLS foci in the SCN-derived pseudopronuclei overlapped well with the signals stained with Hoechst (Figs. 17F, G, and H), and were located immediately adjacent to the signals of EGFP fused to a component of centromeric protein complex, CENP-B (Figs. 17I, J, and K). These data show the highly methylated status of the C/P region in the SCN of 1-cell embryo.

Incomplete reprogramming of DNA methylation in the C/P region of SCNT embryos during preimplantation development

To examine whether the hypermethylation status of SCN C/P region is reprogrammed during preimplantation development, EGFP-MBD-NLS signals in the SCN-derived pseudopronucleus and female pronucleus of 1-cell embryo were monitored by time-lapse imaging (Fig. 18A). Total fluorescent intensity remained at a high level between 4 and 14 h after egg activation (Figs. 18A and B). In addition, bisulfite sequencing analysis revealed that the DNA methylation levels of the major and minor satellites in morulae and blastocysts reconstructed by SCNT are approximately twice as high as those in the embryos produced by IVF (Fig. 18C). No significant difference was found in the methylation level of IAP between the SCNT and IVF embryos.

These results show that the C/P region of the SCNT embryo is specifically resistant to reprogramming of DNA methylation between the 1-cell and blastocyst stages. Thus, the erasure of hypermethylated status of the C/P region during germline cell development (PGC formation) may be required for normal development of the cloned embryos, as described previously (Fulka et al., 2004).

Possible role of DNA hypomethylation in germline cells

The C/P region of major and minor satellites covering approximately 3.5% of whole mouse genome (Waterston et al., 2002) forms a constitutive heterochromatin containing the hypermethylated repeat sequences (Lehnertz et al., 2003). However, little is known about the biological significance of the germline-specific, extensive hypomethylation. I assume that the hypomethylation status may be associated with germ cell-specific gene expression. Since at least 28 transcriptional units present in the pericentric region are highly expressed in the testis and ovary (She et al., 2004), the hypomethylation status of germline cells (Figs. 14, 15, and 16) may reflect a unique architecture of the centromere and affect gene expression. Alternatively, it is possible that the hypomethylated C/P region may contribute to the germ-cell specific chromosomal segregation, meiosis. If so, the hypomethylated satellites may function as a key regulator for the assembly of certain molecules specific for the meiotic chromosomes to the kinetochore.

This study opens the door to a new insight into the epigenetic divergence between germ and somatic cells. Recently, germ cell-like cells have been established from non-germline cells, such as ES cells (Hubner et al., 2003; Toyooka et al., 2003) and bone marrow cells (Johnson et al., 2005).

Analysis of the methylation status in the C/P region of “germ-cell like” cells will give us important information on the definition of “germ cells.” Moreover, further works on the molecular mechanism controlling the DNA methylation of the C/P region are necessary for defining the centromere function(s) in germline, and for elucidating the differentiation mechanisms of the germ and somatic cell lineages.

GENERAL CONCLUSION

This study raises the possibility that the nuclear architecture or mobility of nucleoprotein may play a role(s) in regulation of embryonic development in the mouse. When FRAP analysis of preimplantation embryos was carried out, the mobility of HP1β in the nuclear euchromatin region was decreased in the 4-cell embryos compared with the 1-cell embryos (Chapter I). These results suggest that the chromatin stability may increase as the embryo develops, and other nucleoproteins such as histone may also mobilize dynamically in the early embryos in a similar manner. In Chapter II, retrospective analysis indicated that the localization of methylated DNA in the male pronucleus of 1-cell embryos may be correlated with preimplantation development. It is also possible that the nuclear architecture may affect preimplantation development. The chromatin architecture is presumably regulated by a higher-order epigenetic information different from epigenetic modifications including DNA methylation, histone methylation, and acetylation. Finally, I showed that the C/P region is hypomethylated in various germ cells including preimplantation embryos, male germ cell, GS cells, and mGS cells (Chapter III). The SCNT embryos showed the hypermethylated status in the C/P region compared with the normally fertilized embryos. Thus, the hypomethylation status of the C/P region may be involved in the germ cell-specific events such as meiosis. Overall, the integration of additional information on epigenetic regulations will be valuable for understanding the nuclear reprogramming process further.

ACKNOWLEDGEMENTS

I would like to express my gratitude to all those who offered me guidance supports and encouragement during the preparation of this doctoral thesis.

First of all, I would like to express my sincere appreciation to Professor Tadashi Baba for all his supports and guidance throughout my research work. I wish to express my deep thanks to Drs. Kazuo Yamagata and Shin-ichi Kashiwabara for their support and encouragement. I also thank all members of our laboratory, especially Dr. Tomoko Nakanishi for her technical supports and assistance. Moreover, I wish to express my sincere appreciation to Drs. Kuniya Abe and Satoru Kobayakawa for technical assistance for FRAP analysis. I would express my profound gratitude to Dr. Takashi Shinohara providing GS and mGS cells. I am deeply grateful to Drs. Atsuo Ogura, Kimiko Inoue, and Hiromi Miki and Mses. Narumi Ogonuki and Michiko Hirose for providing PGC, embryo body of mGS cell and SCNT embryos. Finally, I would like to give my special thanks to all my family, my father (Mr. Hiroshi Y.), mother (Mrs. Yoko Y.), younger brother (Mr. Yuga Y.) for their supports.

REFERENCES

Aoki, F., Worrad, D. M., Schultz, R. M., 1997. Regulation of transcriptional activity during the first and second cell cycles in the preimplantation mouse embryo. *Dev. Biol*. 181, 296-307.

Arney, K. L., Bao, S., Bannister, A. J., Kouzarides, T., and Surani, M. A., 2002. Histone methylation defines epigenetic asymmetry in the mouse zygote. *Int. J. Dev. Biol*. 46, 317-320.

Bannister AJ, Zegerman P, Partridge JF, Miska EA, Thomas JO, Allshire RC, Kouzarides T., 2001 Selective recognition of methylated lysine 9 on histone H3 by the HP1 chromodomain. *Nature* 410, 120-124.

Beaujean, N., Taylor, J., Gardner, J., Wilmut, I., Meehan, R., and Young, L., 2004. Effect of limited DNA methylation reprogramming in the normal sheep embryo on somatic cell nuclear transfer. *Biol. Reprod*. 71, 185-193.

Bernardino-Sgherri, J., Chicheportiche, A., Niveleau, A., Dutrillaux, B., 2002. Unusual chromosome cleavage dynamic in rodent neonatal germ cells. *Chromosoma* 111, 341-347.

Bernard P, Maure JF, Partridge JF, Genier S, Javerzat JP, Allshire RC., 2001. Requirement of heterochromatin for cohesion at centromeres. *Science* 294, 2539-2542.

Bouniol, C., Nguyen, E., Debey, P., 1995. Endogenous Transcription Occurs at the 1-Cell Stage in the Mouse Embryo. *Exp. Cell Res*. 218, 57-62.

Campbell RE, Tour O, Palmer AE, Steinbach PA, Baird GS, Zacharias DA, Tsien RY., 2002. A monomeric red fluorescent protein. *Proc. Natl. Acad. Sci. USA*. 99, 7877-7882.

Chatot, C. L., Ziomek, C. A., Bavister, B. D., Lewis, J. L., and Torres, I., 1989.

An improved culture medium supports development of random-bred 1-cell mouse embryos *in vitro*. *J. Reprod. Fertil*. 86, 679-688.

Cheutin T, McNairn AJ, Jenuwein T, Gilbert DM, Singh PB, Misteli T., 2003. Maintenance of stable heterochromatin domains by dynamic HP1 binding. *Science* 299, 721-725.

Coffigny, H., Bourgeois, C., Ricoul, M., Bernardino, J., Vilain, A., Niveleau, A., Malfoy, B., and Dutrillaux, B., 1999. Alterations of DNA methylation patterns in germ cells and Sertoli cells from developing mouse testis. *Cytogenet. Cell Genet.* 87, 175-181.

Cowell, I. G., Aucott, R., Mahadevaiah, S. K., Burgoyne, P. S., Huskisson, N., Bongiorni, S., Prantera, G., Fanti, L., Pimpinelli, S., Wu, R., Gilbert, D. M., Shi, W., Fundele, R., Morrison, H., Jeppesen, P., and Singh, P. B., 2002. Heterochromatin, HP1 and methylation at lysine 9 of histone H3 in animals. *Chromosoma* 111, 22-36.

Cremer, T., and Cremer, C., 2001. Chromosome territories, nuclear architecture and gene regulation in mammalian cells. *Nat. Rev. Genet.* 2, 292-301.

Dean, W., Santos, F., Stojkovic, M., Zakhartchenko, V., Walter, J., Wolf, E., and Reik, W., 2001. Conservation of methylation reprogramming in mammalian development: aberrant reprogramming in cloned embryos. *Proc. Natl. Acad. Sci. USA.* 98, 13734-13738.

Doherty, A. S., Bartolomei, M. S., Schultz, R. M. 2002 Regulation of stage-specific nuclear translocation of Dnmt1o during preimplantation mouse development. *Dev. Biol.* 242, 255-266.

Dozortsev, D., Coleman, A., Nagy, P., Diamond, M. P., Ermilov, A., Weier, U., Liyanage, M., and Reid, T., 2000. Nucleoli in a pronuclei-stage mouse embryo are represented by major satellite DNA of interconnecting

chromosomes. *Fertil. Steril.* 73, 366-371.

Extavour, C.G., Akam, M., 2003. Mechanisms of germ cell specification across the metazoans: epigenesis and preformation. *Development* 130, 5869-5884.

Ferguson-Smith, A. C., and Surani, M. A., 2001. Imprinting and the epigenetic asymmetry between parental genomes. *Science* 293, 1086-1089.

Festenstein R, Pagakis SN, Hiragami K, Lyon D, Verreault A, Sekkali B, Kioussis D., 2003. Modulation of heterochromatin protein 1 dynamics in primary mammalian cells. *Science* 299, 719-721.

Fischle W, Tseng BS, Dormann HL, Ueberheide BM, Garcia BA, Shabanowitz J, Hunt DF, Funabiki H, Allis CD., 2005. Regulation of HP1-chromatin binding by histone H3 methylation and phosphorylation. *Nature* 438, 1116-1122.

Fujita, N., Takebayashi, S., Okumura, K., Kudo, S., Chiba, T., Saya, H., and Nakao, M., 1999. Methylation-mediated transcriptional silencing in euchromatin by methyl-CpG binding protein MBD1 isoforms. *Mol. Cell. Biol.* 19, 6415-6426.

Fujita, N., Shimotake, N., Ohki, I., Chiba, T., Saya, H., Shirakawa, M., and Nakao, M., 2000. Mechanism of transcriptional regulation by methyl-CpG binding protein MBD1. *Mol. Cell. Biol*. 20, 5107-5118.

Fujita, N., Watanabe, S., Ichimura, T., Tsuruzoe, S., Shinkai, Y., Tachibana, M., Chiba, T., and Nakao, M., 2003. Methyl-CpG binding domain 1 (MBD1) interacts with the Suv39h1-HP1 heterochromatic complex for DNA methylation-based transcriptional repression. *J. Biol. Chem*. 278, 24132-24138.

Fulka, J., Jr., Miyashita, N., Nagai, T., and Ogura, A., 2004. Do cloned

mammals skip a reprogramming step? Nat. Biotechnol. 22, 25-26.

Gasser, S. M., 2002. Visualizing chromatin dynamics in interphase nuclei. *Science* 296, 1412-1416.

Guenatri, M., Bailly, D., Maison, C., Almouzni, G., 2004. Mouse centric and pericentric satellite repeats form distinct functional heterochromatin. *J. Cell Biol.* 166, 493-505.

Haaf, T., and Ward, D. C., 1995. Higher order nuclear structure in mammalian sperm revealed by in situ hybridization and extended chromatin fibers. *Exp. Cell Res.* 219, 604-611.

Hajkova, P., Erhardt, S., Lane, N., Haaf, T., El-Maarri, O., Reik, W., Walter, J., Surani, M.A., 2002. Epigenetic reprogramming in mouse primordial germ cells. *Mech. Dev.* 117, 15-23.

Hamatani, T., Carter, M. G., Sharov, A. A., and Ko, M. S., 2004. Dynamics of global gene expression changes during mouse preimplantation development. *Dev. Cell* 6, 117-131.

Heard E., 2004. Recent advances in X-chromosome inactivation. *Curr Opin Cell Biol*. 16, 247-255.

Hirota T, Lipp JJ, Toh BH, Peters JM., 2005. Histone H3 serine 10 phosphorylation by Aurora B causes HP1 dissociation from heterochromatin. *Nature* 438, 1176-1180.

Howell, C. Y., Bestor, T. H., Ding, F., Latham, K. E., Mertineit, C., Trasler, J. M., Chaillet, J. R. 2001. Genomic imprinting disrupted by a maternal effect mutation in the Dnmt1 gene. *Cell* 104, 829-838.

Hubner, K., Fuhrmann, G., Christenson, L.K., Kehler, J., Reinbold, R., De La Fuente, R., Wood, J., Strauss, J.F. III, Boiani, M., Scholer, H.R., 2003. Derivation of oocytes from mouse embryonic stem cells. *Science* 300, 1251-1256.

Johnson, J., Bagley, J., Skaznik-Wikiel, M., Lee, H.-J., Adams, G.B., Niikura, Y., Tschudy, K.S., Tilly, J.C., Cortes, M.L., Forkert, R., Spitzer, T., Iacomini, J., Scadden, D.T., Tilly, J.L., 2005. Oocyte generation in adult mammalian ovaries by putative germ cells in bone marrow and peripheral blood. Cell 122, 303-315.

Jones, P. A., and Takai, D., 2001. The role of DNA methylation in mammalian epigenetics. *Science* 293, 1068-1070.

Jones, P. L., Veenstra, G. J., Wade, P. A., Vermaak, D., Kass, S. U., Landsberger, N., Strouboulis, J., and Wolffe, A. P., 1998. Methylated DNA and MeCP2 recruit histone deacetylase to repress transcription. *Nat. Genet*. 19, 187-191.

Jorgensen, H. F., Adie, K., Chaubert, P., and Bird, A. P., 2006. Engineering a high-affinity methyl-CpG-binding protein. *Nucl. Acids Res.* 34, e96.

Kanatsu-Shinohara, M., Inoue, K., Lee, J., Yoshimoto, M., Ogonuki, N., Miki, H., Baba, S., Kato, T., Kazuki, Y., Toyokuni, S., Toyoshima, M., Niwa, O., Oshimura, M., Heike, T., Nakahata, T., Ishino, F., Ogura, A., Shinohara, T., 2004. Generation of pluripotent stem cells from neonatal mouse testis. Cell 119, 1001-1012.

Kanatsu-Shinohara, M., Ogonuki, N., Inoue, K., Miki, H., Ogura, A., Toyokuni, S., Shinohara, T., 2003. Long-term proliferation in culture and germline transmission of mouse male germline stem cells. Biol. Reprod. 69, 612-616.

Kanda T, Sullivan KF, Wahl GM., 1998. Histone-GFP fusion protein enables sensitive analysis of chromosome dynamics in living mammalian cells. *Curr Biol*. 8, 377-385.

Kang, Y. K., Koo, D. B., Park, J. S., Choi, Y. H., Chung, A. S., Lee, K. K., and Han, Y. M., 2001. Aberrant methylation of donor genome in cloned

bovine embryos. *Nat. Genet*. 28, 173-177.

Kashiwabara, S., Noguchi, J., Zhuang, T., Ohmura, K., Honda, A., Sugiura, S., Miyamoto, K., Takahashi, S., Inoue, K., Ogura, A., Baba, T., 2002. Regulation of spermatogenesis by testis-specific, cytoplasmic poly(A) polymerase TPAP. Science 298, 1999-2002.

Kato, Y., Kaneda, M., Hata, K., Kumaki, K., Hisano, M., Kohara, Y., Okano, M., Li, E., Nozaki, M., 2007. Role of the Dnmt3 family in *de novo* methylation of imprinted and repetitive sequences during male germ cell development in the mouse. Hum. Mol. Genet. 16, 2272-2280.

Kim, E., Nishimura, H., Iwase, S., Yamagata, K., Kashiwabara, S., and Baba, T., 2004. Synthesis, processing, and subcellular localization of mouse ADAM3 during spermatogenesis and epididymal sperm transport. *J Reprod Dev*. 50, 571-578.

Kimura, Y., and Yanagimachi, R., 1995a. Intracytoplasmic sperm injection in the mouse. *Biol. Reprod*. 52, 709-720.

Kimura, Y., and Yanagimachi, R., 1995b. Mouse oocytes injected with testicular spermatozoa or round spermatids can develop into normal offspring. *Development* 121, 2397-2405.

Kishigami, S., Van Thuan, N., Hikichi, T., Ohta, H., Wakayama, S., Mizutani, E., and Wakayama, T., 2006. Epigenetic abnormalities of the mouse paternal zygotic genome associated with microinsemination of round spermatids. *Dev. Biol*. 289, 195-205.

Kobayakawa S, Miike K, Nakao M, Abe K., 2007. Dynamic changes in the epigenomic state and nuclear organization of differentiating mouse embryonic stem cells. *Genes Cells* 12, 447-460.

Kurotaki, Y., Hatta, K., Nakao, K., Nabeshima, Y., Fujimori, T. 2007 Blastocyst axis is specified independently of early cell lineage but aligns with

the ZP shape. *Science.* 316, 719-723.

Lachner M, O'Carroll D, Rea S, Mechtler K, Jenuwein T., 2001. Methylation of histone H3 lysine 9 creates a binding site for HP1 proteins. *Nature* 410, 116-120.

Lawitts, J. A., and Biggers, J. D., 1993. Culture of preimplantation embryos. *Methods Enzymol*. 225, 153-164.

Lehnertz B, Ueda Y, Derijck AA, Braunschweig U, Perez-Burgos L, Kubicek S, Chen T, Li E, Jenuwein T, Peters AH., 2003. Suv39h-mediated histone H3 lysine 9 methylation directs DNA methylation to major satellite repeats at pericentric heterochromatin. *Curr Biol*. 13, 1192-1200.

Li, E., 2002. Chromatin modification and epigenetic reprogramming in mammalian development. *Nat. Rev. Genet*. 3, 662-673.

Mager, J., Bartolomei, M. S. 2005. Strategies for dissecting epigenetic mechanisms in the mouse. *Nat. Genet*. 37, 1194-1200.

Marchal, R., Chicheportiche, A., Dutrillaux, B., and Bernardino-Sgherri, J., 2004. DNA methylation in mouse gametogenesis. *Cytogenet. Genome Res.* 105, 316-324.

Martens JH, O'Sullivan RJ, Braunschweig U, Opravil S, Radolf M, Steinlein P, Jenuwein T., 2005. The profile of repeat-associated histone lysine methylation states in the mouse epigenome. *EMBO J.* 24, 800-812.

Martin, C., Beaujean, N., Brochard, V., Audouard, C., Zink, D., and Debey, P., 2006. Genome restructuring in mouse embryos during reprogramming and early development. *Dev. Biol.* 292, 317-332.

Mayer, W., Niveleau, A., Walter, J., Fundele, R., and Haaf, T., 2000. Demethylation of the zygotic paternal genome. *Nature* 403, 501-502.

McGrath, J., Solter, D. 1983. Nuclear transplantation in the mouse embryo by

microsurgery and cell fusion. *Science.* 220, 1300-1302.

McLaren, A., 1994. Germline and soma: interactions during early mouse development. Semin. Dev. Biol. 5, 43-49.

Meshorer E, Yellajoshula D, George E, Scambler PJ, Brown DT, Misteli T., 2006. Hyperdynamic plasticity of chromatin proteins in pluripotent embryonic stem cells. *Dev Cell* 10, 105-116.

Mikami Y, Hori T, Kimura H, Fukagawa T., 2005. The functional region of CENP-H interacts with the Nuf2 complex that localizes to centromere during mitosis. *Mol Cell Biol*. 25, 1958-1970.

Miki, H., Inoue, K., Kohda, T., Honda, A., Ogonuki, N., Yuzuriha, M., Mise, N., Matsui, Y., Baba, T., Abe, K., Ishino, F., Ogura, A., 2005. Birth of mice produced by germ cell nuclear transfer. Genesis 41, 81-86.

Ng, H. H., Bird, A. 1999. DNA methylation and chromatin modification. *Curr. Opin. Genet. Dev.* 9, 158-163

Ogura, A., Ogonuki, N., Takano, K., and Inoue, K., 2001. Microinsemination, nuclear transfer, and cytoplasmic transfer: the application of new reproductive engineering techniques to mouse genetics. *Mamm. Genome* 12, 803-812.

Ogura, A., Yanagimachi, R., 1993. Round spermatid nuclei injected into hamster oocytes from pronuclei and participate in syngamy. Biol. Reprod. 48, 219-225.

Ogonuki, N., Inoue, K., Yamamoto, Y., Noguchi, Y., Tanemura, K., Suzuki, O., Nakayama, H., Doi, K., Ohtomo, Y., Satoh, M., Nishida, A., Ogura, A., 2002. Early death of mice cloned from somatic cells. Nat. Genet. 30, 253-254.

Ohinata, Y., Payer, B., O'Carroll, D., Ancelin, K., Ono, Y., Sano, M., Barton, S.C., Obukhanych, T., Nussenzweig, M., Tarakhovsky, A., Saitou, M.,

Surani, M.A., 2005. Blimp1 is a critical determinant of the germ cell lineage in mice. Nature 436, 207-213.

Peters AH, O'Carroll D, Scherthan H, Mechtler K, Sauer S, Schofer C, Weipoltshammer K, Pagani M, Lachner M, Kohlmaier A, Opravil S, Doyle M, Sibilia M, Jenuwein T., 2001. Loss of the Suv39h histone methyltransferases impairs mammalian heterochromatin and genome stability. *Cell* 107, 323-337.

Phair RD, Misteli T., 2000. High mobility of proteins in the mammalian cell nucleus. *Nature* 404, 604-609.

Pittoggi, C., Renzi, L., Zaccagnini, G., Cimini, D., Degrassi, F., Giordano, R., Magnano, A. R., Lorenzini, R., Lavia, P., and Spadafora, C., 1999. A fraction of mouse sperm chromatin is organized in nucleosomal hypersensitive domains enriched in retroposon DNA. *J. Cell Sci.* 112, 3537-3548.

Plusa, B., Hadjantonakis, A. K., Gray, D., Piotrowska-Nitsche, K., Jedrusik, A., Papaioannou, V. E., Glover, D. M., Zernicka-Goetz, M. 2005 The first cleavage of the mouse zygote predicts the blastocyst axis. *Nature*. 434, 391-395.

Ratnam, S., Mertineit, C., Ding, F., Howell, C. Y., Clarke, H. J., Bestor, T. H., Chaillet, J. R., Trasler, J. M. 2002. Dynamics of Dnmt1 methyltransferase expression and intracellular localization during oogenesis and preimplantation development. *Dev. Biol.* 245, 304-314.

Razin, A., Riggs, A. D. 1980. DNA methylation and gene function. *Science* 210, 604-610.

Reik, W., Dean, W., and Walter, J., 2001. Epigenetic reprogramming in mammalian development. *Science* 293, 1089-1093.

Sanford, J., Forrester, L., Chapman, V., Chandley, A., Hastie, N., 1984.

Methylation patterns of repetitive DNA sequences in germ cells of *Mus musculus*. Nucl. Acids Res. 12, 2823-2836.

Santos, F., Hendrich, B., Reik, W., and Dean, W., 2002. Dynamic reprogramming of DNA methylation in the early mouse embryo. *Dev. Biol*. 241, 172-182.

Santos, F., Peters, A. H., Otte, A. P., Reik, W., and Dean, W., 2005. Dynamic chromatin modifications characterise the first cell cycle in mouse embryos. *Dev. Biol*. 280, 225-236.

Sarraf, S. A., and Stancheva, I., 2004. Methyl-CpG binding protein MBD1 couples histone H3 methylation at lysine 9 by SETDB1 to DNA replication and chromatin assembly. *Mol. Cell* 15, 595-605.

Schatten, G., Simerly, C., Palmer, D. K., Margolis, R. L., Maul, G., Andrews, B. S., and Schatten, H., 1988. Kinetochore appearance during meiosis, fertilization and mitosis in mouse oocytes and zygotes. *Chromosoma* 96, 341-352.

Schaufele, F., Enwright, J. F., 3rd, Wang, X., Teoh, C., Srihari, R., Erickson, R., MacDougald, O. A., and Day, R. N., 2001. CCAAT/enhancer binding protein alpha assembles essential cooperating factors in common subnuclear domains. *Mol. Endocrinol*. 15, 1665-1676.

Seki, Y., Hayashi, K., Itoh, K., Mizugaki, M., Saitou, M., Matsui, Y., 2005. Extensive and orderly reprogramming of genome-wide chromatin modifications associated with specification and early development of germ cells in mice. Dev. Biol. 278, 440-458.

She, X., Horvath, J.E., Jiang, Z., Liu, G., Furey, T.S., Christ, L., Clark, R., Graves, T., Gulden, C.L., Alkan, C., Bailey, J.A., Sahinalp, C., Rocchi, M., Haussler, D., Wilson, R.K., Miller, W., Schwartz, S., Eichler, E.E., 2004. The structure and evolution of centromeric transition regions

within the human genome. Nature 430, 857-864.

Shelby, R. D., Hahn, K. M., and Sullivan, K. F., 1996. Dynamic elastic behavior of alpha-satellite DNA domains visualized in situ in living human cells. *J. Cell Biol*. 135, 545-557.

Shi, W., and Haaf, T., 2002. Aberrant methylation patterns at the two-cell stage as an indicator of early developmental failure. *Mol. Reprod. Dev*. 63, 329-334.

Shiota, K., Kogo, Y., Ohgane, J., Imamura, T., Urano, A., Nishino, K., Tanaka, S., Hattori, N., 2002. Epigenetic marks by DNA methylation specific to stem, germ and somatic cells in mice. Genes Cells 7, 961-969.

Tamashiro, K.L.K., Wakayama, T., Akutsu, H., Yamazaki, Y., Lachey, J.L., Wortman, M.D., Seeley, R.J., D'Alessio, D.A., Woods, S. C., Yanagimachi, R., Sakai, R.R., 2002. Cloned mice have an obese phenotype not transmitted to their offspring. Nat. Med. 8, 262-267.

Toyoda, Y., Yokoyama, M., and Hoshi, T., 1971. Studies on fertilization of mouse eggs *in vitro*. I. *In vitro* fertilization of eggs by fresh epididymal sperm. *Jpn. J. Anim. Reprod*. 16, 147-151.

Toyooka, Y., Tsunekawa, N., Akasu, R., Noce, T., 2003. Embryonic stem cells can form germ cells *in vitro*. Proc. Natl. Acad. Sci. USA 100, 11457-11462.

Tsunoda, Y., Yasui, T., Shioda, Y., Nakamura, K., Uchida, T., Sugie, T. 1987. Full-term development of mouse blastomere nuclei transplanted into enucleated two-cell embryos. *J. Exp. Zool.* 242, 147-151.

Wakayama, T., Perry, A. C., Zuccotti, M., Johnson, K. R., Yanagimachi, R. 1998. Full-term development of mice from enucleated oocytes injected with cumulus cell nuclei. *Nature.* 394, 369-374.

Wakayama, T., Yanagimachi, R., 1999. Cloning of male mice from adult tail-tip cells. Nat. Genet. 22, 127-128.

Waterston, R.H., *et al*., 2002. Initial sequencing and comparative analysis of the mouse genome. Nature 420, 520-562.

Wilmut, I., Schnieke, A. E., McWhir, J., Kind, A. J., Campbell, K. H. 1997. Viable offspring derived from fetal and adult mammalian cells. *Nature*. 385, 810-813.

Yamagata, K., Yamazaki, T., Yamashita, M., Hara, Y., Ogonuki, N., and Ogura, A., 2005. Noninvasive visualization of molecular events in the mammalian zygote. *Genesis* 43, 71-79.

Yamazaki T, Yamagata K, Baba T., 2007. Time-lapse and retrospective analysis of DNA methylation in mouse preimplantation embryos by live cell imaging. *Dev Biol*. 304, 409-419.

Yanagimachi, R., 1994. Mammalian fertilization. In *The Physiology of Reproduction* (ed. E. Knobil and J. D. Neill), pp. 189-317. New York: Raven Press.